THE EFFECTS OF pH AND CONCENTRATION ON THE RHEOLOGY OF CARBOPOL GELS

by

Iris Gutowski
BSc, McGill University, 2008

THESIS SUBMITTED IN PARTIAL FULFILLMENT OF
THE REQUIREMENTS FOR THE DEGREE OF

MASTER OF SCIENCE

In the
Department of Physics

SIMON FRASER UNIVERSITY

Summer 2010

APPROVAL

Name:	**Iris Gutowski**
Degree:	**Master of Science**
Title of Thesis:	**The Effects of pH and Concentration on the Rheology of Carbopol Gels**

Examining Committee:

Dr. Michael Plischke, Professor
Chair

_____

Dr. Barbara J. Frisken, Professor
Senior Supervisor

_____

Dr. John L. Bechhoefer, Professor
Supervisor

_____

Dr. Malcolm P. Kennett, Assistant Professor
Supervisor

_____

Dr. Nancy R. Forde, Assistant Professor
Internal Examiner

Date Defended/Approved: August 23rd, 2010

Declaration of
Partial Copyright Licence

ABSTRACT

Rheological measurements were performed on samples of highly cross-linked polymer microgels (Carbopols ETD 2050 and Ultrez 10), at various concentrations and pH values. Dramatic increases at low pH followed by broad peaks at intermediate pH in both yield stress and the elastic modulus were observed across all concentrations studied. We argue that this corresponds to the onset of jamming due to a rapid increase of volume fraction caused by the osmotic swelling of the polyelectrolyte microgel particles in the presence of NaOH. Differences were observed in the yield-stress scaling behaviour between higher and lower concentration samples, which we believe to be indicative of a transition from a percolated structure at low concentrations, to a space filling network of compressed particles at high concentrations.

Keywords: Microgel; Carbopol; Yield Stress; Viscoelasticity.

EXECUTIVE SUMMARY

This thesis deals with the rheological properties of Carbopol microgel suspensions. Carbopol is a family of microgels, made of highly cross-linked poly(acrylic acid), manufactured for a wide variety of industrial purposes, which include the production of tires, cosmetics, and pharmaceuticals. Due to its characteristic yield-stress behaviour, where flow occurs only above a threshold stress, Carbopol has attracted the attention of many rheologists. It has been used in a wide variety of rheological experiments as a model fluid. However, few attempts have been made to understand its underlying structure. The initial motivation for this project was to understand how the bulk rheological behaviour of Carbopol relates to proposed models of its mesostructure. This work is part of a larger project undertaken by the lab of Barbara Frisken here at Simon Fraser University and the lab of John de Bruyn at the University of Western Ontario, which aims to explain how the micro- and mesostructure of Carbopol change under varying pH and concentrations using a combination of small angle light scattering and rheology. It is widely known that the viscosity of Carbopol drastically increases

upon base titration; however, the underlying mechanism behind this remains not well-understood. By studying the various rheological properties of Carbopol gels under a wide range of pH and concentration combined with light scattering analysis, we hope to uncover the mechanisms behind the origins of the yield stress and viscoelasticity observed in Carbopol.

Light scattering, predominately the work of former graduate student David Lee, has revealed two length scales in a Carbopol ETD 2050 microgel: a smaller one believed to correspond to highly crosslinked regions within the gel particle, and another larger one thought to be indicative of a perimeter of looser polymer coils. The smaller length scale was found to remain relatively unchanged over a wide range of concentrations and pH, while the larger length scale was found to drastically increase with small changes in pH.

Rheological properties exhibit some very interesting changes with pH: yield stresses, although existent even in very low concentration low pH samples, were found to drastically increase in magnitude upon reaching pH 4. What is even more interesting is that the yield stress decreases as the pH is increased further. Another quantity of interest, the plateau value of the elastic modulus, also shows a maximum at intermediate pH.

This behaviour suggests that titration with NaOH has competing effects on the rheology of Carbopol: a certain amount of NaOH appears to ‘strengthen’ the material while further base titration appears to ‘weaken’ it. We propose the following explanation for this phenomenon: the addition of small amounts of NaOH leads to an osmotic pressure that causes the particles to swell. Eventually this swelling increases to the point where the particle volume fraction exceeds the limit of random close packing and the particles begin to compress and fill the space, and thereby create an effective network,

which spans the sample. The high volume fraction and compression of the particles increases the degree of jamming within the system and consequently both yield stress and elasticity begin to increase. However, after a critical degree of base titration, the carboxyl groups of the acrylic acid backbone become fully dissociated; with further base titration, the increased presence of sodium ions in the surrounding solution leads to a net inward osmotic pressure, which causes the particles to deswell slightly. This is marked by a drop in both the yield stress and the elastic modulus that is seen in all concentrations.

We also observe a difference in the scaling behaviour of the yield stress and the elastic modulus as functions of pH between the lowest and highest concentration samples. We suggest that this is the result of a transition from a percolated structure at low concentrations, analogous to the case seen in dilute hard spheres, to a volume filling network of compressed particles at higher concentrations.

To Lester, and my parents

ACKNOWLEDGEMENTS

I would like to personally thank all those who have been influential in the production this work. First and foremost, I thank my supervisor Dr. Barbara Frisken, for her continued support and encouragement throughout this project. I would then like to thank, Dr. John de Bruyn at the University of Western Ontario, who generously opened up his rheology laboratory to us for the collection of all bulk rheological data contained in this thesis and also provided invaluable consultation on the analysis and interpretation of our results. I also thank committee members Dr. John Bechhoefer, and Dr. Malcolm Kennett for illuminating many important considerations, and Nancy Forde, for giving her time to read this thesis and to serve as Internal examiner. In addition, I owe my gratitude to former graduate students Dr. Felix Oopong and David Lee for their guidance with the many aspects of the experimentation.

TABLE OF CONTENTS

LIST OF FIGURES

LIST OF TABLES

GLOSSARY

Carbopol	A microgel, composed of crosslinked poly(acrylic acid), developed by B. F. Goodrich. Also known by carbomer, carboxylpolymethylene.
carboxyl group	A functional group of the form COOH.
crosslink	A covalent bond that links one polymer chain to another.
creep	The long timescale deformation of a material under constant stress.
dashpot	A symbol of Newtonian viscous flow, commonly represented by a piston moving in a cylinder.
dissociation	A process in which ionic compounds split into component ions.
elasticity	Reversible stress/strain behaviour.
flow curve	A curve which relates stress to shear rate.
hard spheres	Impenetrable-sphere systems, whose only potential comes from excluded volume interactions.
hydrodynamic radius	The radius of a hypothetical hard sphere that diffuses with the same speed as the particle under examination.
hysteresis	A phenomenon exhibited by a system, in which the behaviour of the system is dependent on its history.

intrinsic viscosity	The limiting value of viscosity as concentration approaches zero.
ionic strength	A measure of the concentration of ions in a solution.
jamming	A restriction of motion in particulate systems, due to the crowding of particles at high volume fraction.
light scattering	A technique to measure the amount of light scattered by a solution over a range of angles. Can be used, for example, to obtain size distributions in particulate systems.
microgel	Small particles of crosslinked polymer of very high molecular weight.
mesostructure	An intermediate level structure within a material, in between micro- and macrostructure.
microrheology	A technique to measure the rheological properties of a material by studying the dynamics of small embedded tracer particles.
percolation	The presence of randomly distributed voids within a structure of connected clusters.
pH	A measure of the acidity or basicity of a solution, it is given by the logarithm of the molar concentration of dissolved hydronium ions.
pK_a	The acid dissociation constant. A quantitative measure of the strength of an acid dispersed in a solution, measured by the pH at which half of all ions become dissociated.
polyelectrolyte	A polymer whose monomer units bear an electrolyte group, or a source of free ions, which dissociate in solution.
radius of gyration	The square root of the ratio of the moment of inertia of a body about a given axis to its mass.
rheology	The study of flow and deformation of materials.
rheometer	An instrument that measures rheological properties.
strain	Deformation relative to a configuration of length. Shear strain, or shear, is the movement of a layer of material relative to parallel adjacent layers.

stress	Force per unit area. Shear stress is the component of the stress parallel to the area considered.
transducer	A sensor used to detect a parameter in one form of energy and report it in another form (usually an electrical and/or digital signal).
thixotropy	The presence of a time-dependent viscosity.
titration	The addition of ions to a solution to bring about a change in pH.
viscosity	A measure of a fluid's resistance to flow.
volume fraction	The volume of a suspension occupied by component particles, divided by the overall volume.
yield stress	The critical value of stress, above which onset of flow occurs.

1: INTRODUCTION

There exist many fluids whose flow cannot be described by the linear response of the Newtonian flow equations. These materials display behaviour that ranges from that of a viscous liquid to that of an elastic solid to some combination of the two; we dub such materials non-Newtonian, or complex fluids. Complex fluids comprise a wide range of materials, many of which we encounter on a daily basis. Typical examples of such fluids include blood, paint, toothpaste, mayonnaise, shaving cream, silly putty, and a variety of others. All of these fluids exhibit some type of unusual response to external forces, in that their viscosities are somehow dependent on the nature of the forces applied to them: some fluids drastically thicken under applied forces, while others flow more freely. One particularly interesting class of complex fluids is the yield-stress fluid; these fluids behave as solids below a certain critical stress and as liquids above it. Many of the above examples of complex fluids exhibit yield-stress behaviour, specifically: mayonnaise, toothpaste, shaving cream, and hair gel. All of these fluids will easily flow from their containers when external force is applied; yet they also maintain their form and cease to

flow when they are subjected to the relatively weak force of gravity. It is this ability of such fluids to hold their shape under low stresses that makes them so useful for a variety of purposes.

Carbopol gels are archetypical yield-stress fluids. Even at remarkably low concentrations, they display both a clear yield stress and a high elasticity. These properties are highly tuneable with both pH and concentration, and yet are relatively insensitive to temperature; thus, they make Carbopol an ideal system for a wide variety of rheological studies. Carbopol has been used to study many problems in fluid dynamics, which range from bubble dynamics, to the settling of particles, to the caverns created by impellers [1-6]. Carbopol is also used for a wide variety of industrial purposes, which range from thickeners for cosmetics and drug delivery systems to industrial lubricants [7,8].

While Carbopol behaves exceptionally well for these practical purposes, little is known about its actual microstructure. This has led us to ask, 'What is it about the structure of this microgel that gives it such high yield stress and elasticity at such low concentrations?' Pondering the aforementioned question leads us to ask an even more basic question: 'What gives any fluid a yield stress?' Surprisingly enough, this exceedingly simple question has no clear answer. The origin and true nature of the yield stresses observed in many complex fluids is a topic still full of contention among experts in the field [9-11]. Some, such as Barnes and Walters, even suggest that there is no such thing as a true yield stress: they argue that a yield stress marks not the transition from liquid to solid, but rather that from viscous liquid to even more viscous liquid [12,13]. To support these claims, they have cited a plateau seen in viscosity curves at low shear

rates, which contrasts the divergence expected of a true yield-stress fluid [13,14]. However, there has been a great deal of recent research, which involves Carbopol and other complex fluids, that has endeavoured to show that true yield-stress fluids indeed exist and that Carbopol gels are ideal examples of such fluids [10,15,16]. Bonn *et al.* have found that the expected divergent behaviour is in fact seen when care is taken to ensure the system is in a steady state, which entails taking measurements at very long time scales [10].

A variety of systems from polymer microgels such as Carbopol, to foams, emulsions, and hard-sphere colloids, are known to possess yield stresses [17,18]. These different systems also display similar viscoelastic frequency responses [19]. One general property that all of these systems share is that they are all examples of particle suspensions. As such, they tend to exist in configurations that are characterized by structural disorder and metastability [20]. Thus, they are prone to glass-like jamming behaviour, whereby neighbouring particles trap and cage each other and thus restrict long-range motion in the system. This behaviour leads to the appearance of long-timescale structural relaxations. These long-timescale relaxations are similar the caged dynamics observed in molecular glasses but differ in that they are initiated predominantly by external shears as opposed to Brownian motion [20]. If the yield stress were simply the result of this type of inter-particle dynamics, a hard-sphere model should suffice to explain the rheological behaviour. However, there appears to be more at play: namely, the elastic properties of the component particles are significant. In many yield-stress systems, particles are soft and deformable, as is the case for the air bubbles and droplets of foams and emulsions, or the spongy particles of a microgel [17]. It seems reasonable

to suggest that the yield stress in such materials is related in some way to the threshold of deformation of these component particles, and that most likely, the yield stress originates from a combination of both glassy particle dynamics and intra-particle elasticity. Cloitre offers the following model for this interplay: concentrated microgels consist of pastes of compressed elastic particles, which jam and cage each other. When low external stress is applied, the individual particles of the paste simply deform and dissipate the energy elastically, while when higher stress is applied the system will undergo structural rearrangements, whereby particles escape their cages and energy is dissipated through flow [21]. Sollich *et al.* have extensively modelled the behaviour of such soft glassy systems; their phenomenological model, dubbed SGR, describes the dynamics of elements confined to cages, which they can escape from by deforming once they are imparted with sufficient activation energy [20]. The model assumes a spatially homogeneous strain rate while it allows for local inhomogeneities in stress and strain [20], which is critical in the description of glassy rheology. The model shows good qualitative agreement with the rheological behaviour observed in Carbopol and other soft glassy systems.

Carbopol is a system uniquely suited to testing these ideas, as the properties of its component particles are readily tuneable. Carbopol was developed in the 1950s in the laboratories of BF Goodrich for use as a thickening agent in tires. Early studies noted the presence of yield-stress behaviour in Carbopol gels that was relatively insensitive to temperature, as well as viscosities that were much higher than those of equivalent linear polymer systems [22]. In the 1970s, Bagley and Taylor studied this viscosity response in Carbopol and similar microgels over a range of concentrations and ionic strengths. They

noted the presence of two distinct regimes of viscosity increase with concentration: at low concentrations, viscosity increased linearly with concentration; then, after a critical concentration, it began to follow a power law [23,24]. In the decades following, multiple groups have studied Carbopol using techniques such as microrheology, light scattering, scanning electron microscopy, and conventional bulk rheology [25-29]. The results of these studies have allowed researchers to paint a picture of the Carbopol microstructure as a collection of deformable sponges, which form an effective network at high concentrations.

Rheological studies of Carbopol and similar microgels have shown that the properties of the gel such as concentration and crosslink density determine where the system behaves on the spectrum between entangled linear polymers and non-interacting hard spheres, with higher crosslink densities and concentrations making the system more like the latter [30,31]. In Figure 1.1, this concept is illustrated. The low crosslinked gel shows a higher yield stress at low concentration, as evidenced by its ability to suspend a low-density sphere, than the higher crosslinked variety. This is because the lower crosslinked microgel is freer to expand and fill the space. However, as the concentration of the microgels are increased the lower crosslinked gel does not make any significant gains in yield stress, while the higher crosslinked variety forms a stable closely packed structure which is capable of suspending a higher density sphere. The formation of a space-spanning structure is critical for the existence of a yield stress and elasticity. Beyond this, more highly crosslinked particles form stronger structures, which is apparent from values of the yield stress and elastic modulus.

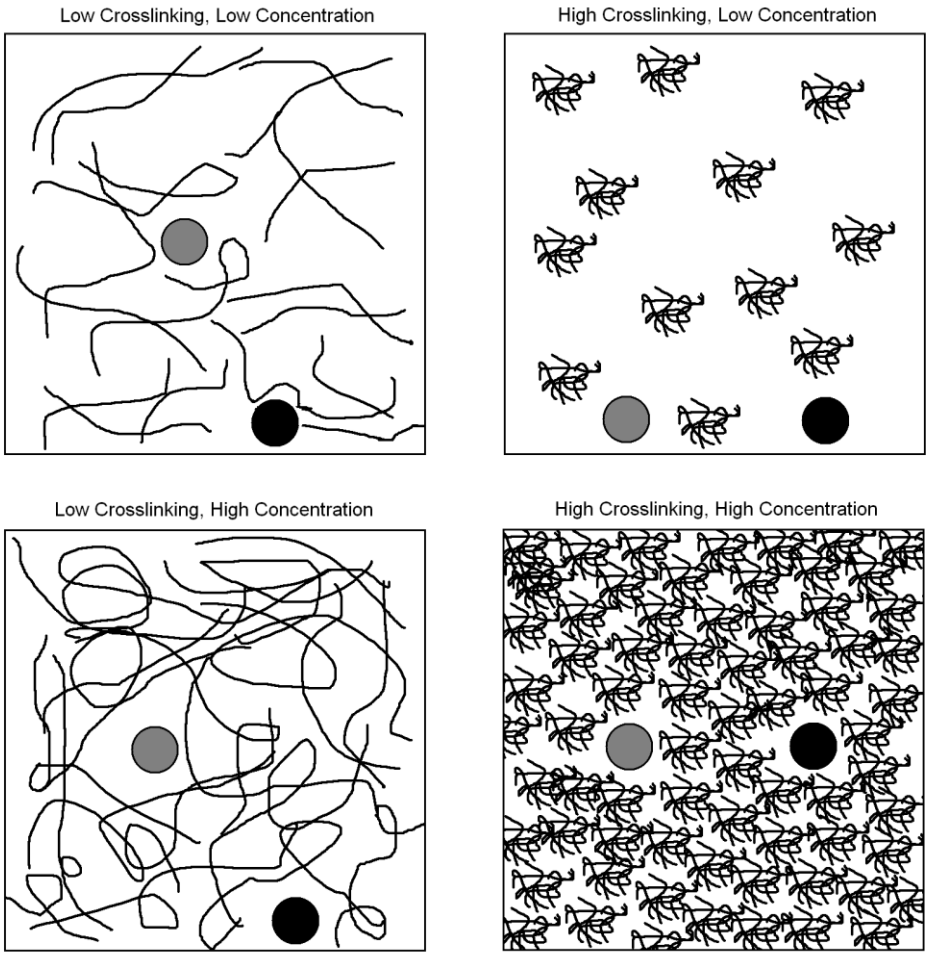

Figure 1.1: Illustration of the effects of crosslinking and concentration on the yield stress of a Carbopol gel [8]. Low density sphere shown in gray, high density sphere shown in black.

It is also been shown that by adjusting the pH of a Carbopol suspension component particle properties can be drastically altered [27]. In the presence of sodium ions, Carbopol's component, particles swell due to a net outward osmotic pressure; this swelling alters particle elasticity along with size through a dilution of the crosslinks within the component particles [25,32].

Many previous studies of Carbopol gels have focused on a range of concentrations in the regime near neutral pH, as this is where viscosity and elasticity tend

to be highest [29,32]. We have found that there is interesting behaviour outside of the confines of this regime, which we feel may lead to better insight into the inner workings of the microgel. Even at very low levels of base titration, we see drastic changes in the rheological properties of Carbopol suspensions: in low concentration samples, yield stresses rapidly appear and then dramatically increase with further titration, and then remain fairly constant until they then begin to drop off in the high end of pH. This suggests that a sufficient particle volume fraction is needed for yield-stress behaviour to be observed and that the existence of a yield stress strongly hinges on the formation of a jammed structure.

In this work, we will present the results of a bulk rheology study the of a comprehensive array of samples as we endeavour to illustrate a more detailed picture of this swelling-elasticity relationship.

2: RHEOLOGY OF COMPLEX FLUIDS

2.1 Introduction

Rheology is the study of flow and deformation. As such, rheologists aim to characterize a material's response to applied forces. There is a wide range of behaviour to be seen in complex fluids. The micro- and meso- scale properties of a system can greatly affect how a system will respond to an applied force. This response may be in the form of an elastic deformation, an irreversible deformation, or as is the case in the fluids we predominantly concern ourselves with, something in between. In fact, all fluids will display effects that are viscoelastic if the timescale of the disturbance is close to an inherent timescale of the material; on very short timescales a fluid will have no time to produce structural rearrangements in response to the external forces and will behave elastically [33].

Understanding the rheology of component materials is crucial for the manufacture and utilization of many industrial and commercial products. Knowledge of rheology is

needed to solve a multitude of problems ranging from drug delivery, to fluid transport, to building safety. The theoretical study of rheology is also a vital field, due to the persistence of many unsolved problems in fluid dynamics and non-equilibrium systems, which have puzzled physicists for centuries.

For a most basic primer on rheology, we can consider the case of a slab of material sheared between two parallel plates: we create shear by applying an external force to the top plate, and we then calculate the resulting strain from the deformation of the material. This example is illustrated in Figure 2.1.1.

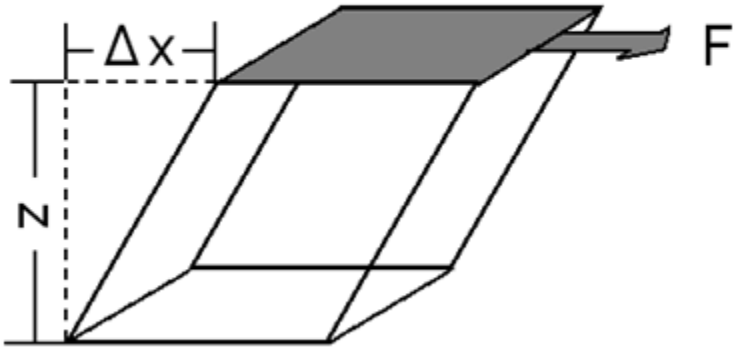

Figure 2.1.1: Simple illustration of shear: A force *F* applied parallel to a slab of height *z*, over an area *A*, results in a stress $\sigma=F/A$, and creates a deformation along the x-axis of Δx, which results in a strain $\gamma=\Delta x/z$.

The strain γ is simply the displacement along the axis of the applied force over the height of the slab. Similarly we can calculate the strain rate $\dot{\gamma}$ by taking the derivative of the strain with respect to time. From this we can determine the relationships between stress and strain rate. For a simple fluid, this is all we need to determine the viscosity η, which is simply the proportionality constant between the two [34]:

$$\sigma = \eta\dot{\gamma}. \tag{2.1.1}$$

To thoroughly study the viscoelastic behaviour observed in complex fluids like Carbopol, we will modify the applied force both by changing its magnitude and by adding a driving frequency. In this chapter we will discuss two important models which help describe much of the observed behaviour seen in Carbopol and other complex fluids.

The first is the Maxwell fluid model, which explains the response of a complex fluid to an oscillatory shear rate. The frequency-dependent behaviour of the Maxwell model has been found to be applicable to a wide variety of complex fluid systems.

The second model is the Herschel-Bulkley model, which is an empirical model that describes the flow of a yield-stress fluid in response to varying shear rates. This model is often used to describe the yield-stress behaviour of Carbopol and other systems [9,27].

After this, we will introduce the concept of jamming, which plays an important role in a variety of complex fluids. We will consider the specific case of jamming in foams and emulsions, as the rheology of these systems is similar to that of microgels and has been studied quite extensively. We will also discuss a theoretical model, known as Soft Glassy Rheology (SGR), which was developed by Sollich *et al.* to explain the jamming behaviour seen in these systems.

2.2 The Maxwell Fluid Model

When examining the rheological properties of a complex system, it is useful to first consider the cases of two ideal substances: Newtonian fluids and Hookean solids, both of which display linear responses to applied shear rates. A Newtonian fluid is a fluid that readily flows in response to applied strains in order to dissipate energy. This flow is proportional to the shear rate and will be out of phase with the applied strain by $\pi/2$ radians. The proportionality constant between the stress σ and the shear rate $\dot{\gamma}$ for a Newtonian fluid is the viscosity η, as shown in Equation 2.1.1. For a Hookean solid the stress is proportional to the applied shear strain where the constant of proportionality is the elastic modulus G [34]:

$$\sigma = G\gamma. \tag{2.2.1}$$

In this case, a small strain will give rise to a large stress that is in phase with the applied strain.

Viscoelastic materials display properties that fall somewhere in between the two extremes of Newtonian liquids and Hookean solids. This is likely due to their micro- and mesoscale structure. A good starting point for examining the rheological properties of viscoelastic fluids is the Maxwell fluid model. In this model, the shear rates of a Newtonian fluid and a Hookean solid are added in series as shown in the circuit diagram in Figure 2.2.1, where the elastic component is represented by a resistor or spring and the viscous component by a dashpot.

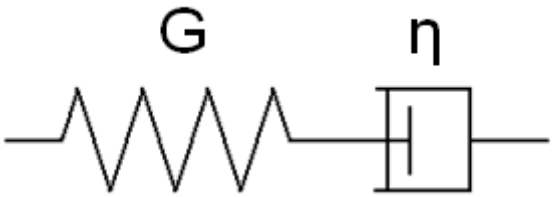

Figure 2.2.1: Circuit diagram of the Maxwell Fluid.

This model leads to a shear rate of the form shown below [34]:

$$\dot{\gamma} = \frac{\dot{\sigma}}{G} + \frac{\sigma}{\eta}. \tag{2.2.2}$$

To analyze the viscoelastic response of such a fluid, we assume the shear rate is an oscillatory function of the basic form shown below:

$$\gamma^*(t) = \gamma_0 e^{i\omega t}. \tag{2.2.3}$$

We also assume that the resulting stress shares the same form:

$$\sigma^*(t) = \sigma_0 e^{i\omega t}. \tag{2.2.4}$$

For a perfect elastic solid, the stress response is in phase with the applied shear, while for a perfect viscous liquid the stress response is out of phase by π/2, so a Maxwell fluid will have a phase angle between zero and π/2 [33]. By substituting Equations 2.2.3 and 2.2.4 into Equation 2.2.2 and taking derivatives we obtain:

$$i\omega\gamma^* = \frac{i\omega\sigma^*}{G} + \frac{\sigma^*}{\eta}, \tag{2.2.5}$$

which then simplifies to:

$$\frac{G\gamma^*}{\sigma^*} = 1 + \frac{G}{i\omega\eta}. \tag{2.2.6}$$

Now, by applying Equation 2.2.1 we obtain an expression for the frequency dependent, complex viscoelastic modulus of the combined system $G^*(\omega)$ (not to be confused with G the constant elastic modulus of the solid component):

$$\frac{G}{G^*(\omega)} = 1 + \frac{1}{i\omega\tau}, \tag{2.2.7}$$

where the decay time τ is the ratio of the viscosity to the elastic modulus as shown below:

$$\tau = \frac{\eta}{G}. \tag{2.2.8}$$

Now we can rewrite the expression for the complex viscoelastic modulus in order to separate out the real and imaginary components as seen below [34]:

$$G^*(\omega) = G'(\omega) + iG''(\omega). \tag{2.2.9}$$

Where,

$$G'(\omega) = \frac{G(\omega\tau)^2}{1 + (\omega\tau)^2}, \tag{2.2.10}$$

and

$$G''(\omega) = \frac{G\omega\tau}{1 + (\omega\tau)^2}. \tag{2.2.11}$$

The moduli are related by causality as described by the Kramers-Kronig relations; they both can be obtained by taking the Fourier transform of the time dependent elastic modulus $G(t)$ [33]. For a Maxwell fluid,

$$G(t) = Ge^{-\frac{t}{\tau}}. \tag{2.2.12}$$

From Equations 2.2.10 and 2.2.11, we can see that $G''(\omega)$ should have a maximum where $\omega=1/\tau$, at which point it also becomes equal to the storage modulus $G'(\omega)$. A plot of the moduli, which illustrates this behaviour, is shown in Figure 2.2.2.

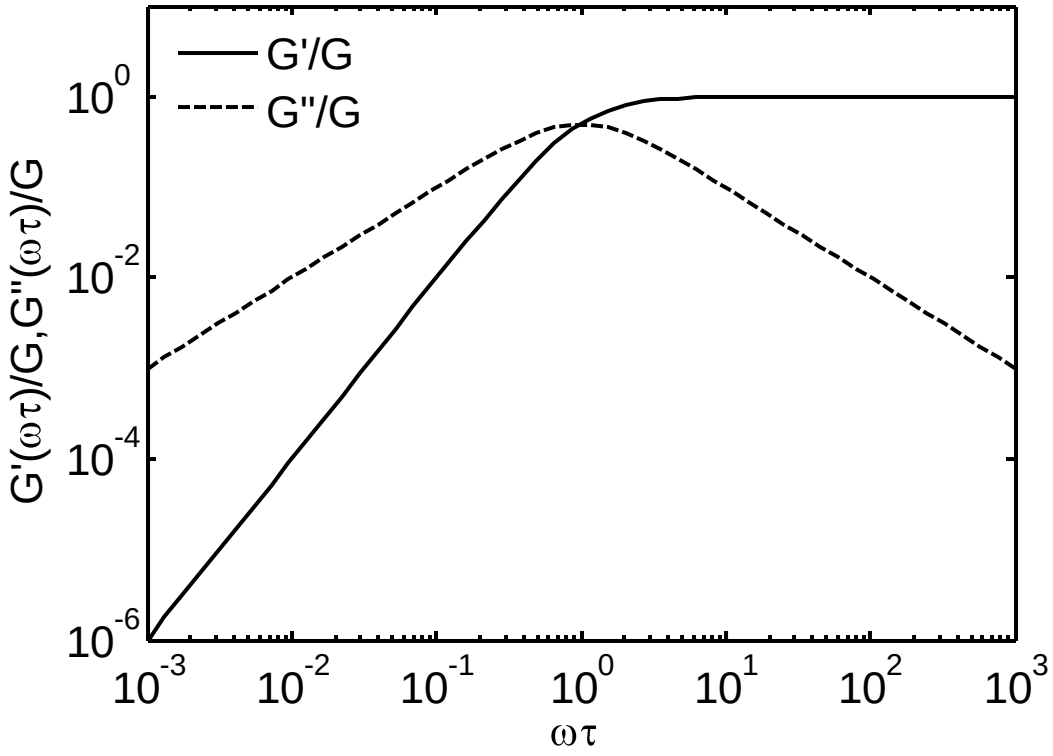

Figure 2.2.2: Plot of the viscoelastic moduli *G'*, and *G"* of a Maxwell fluid as functions of frequency.

The characteristic maximum seen in Figure 2.2.2 is seen in the low frequency behaviour of Carbopol as well as a variety of other yield-stress fluids [17,27]. Looking back at Equations 2.2.10 and 2.2.11, note that in the limit of small frequency the viscous modulus *G*" becomes approximately equal to $\omega\eta$, whereas in the limit of high frequency the elastic modulus *G*' becomes equal to *G*. Thus for small ω and the system behaves effectively as a viscous liquid, while for large ω it behaves as an elastic solid [35].

Most real systems do not display exact Maxwell behaviour, with a single clearly defined relaxation mode. In order to better model such systems, more complex circuit combinations of springs and dashpots can be created. One such model developed to

model the behaviour of concentrated linear polymer melts is the Marvin-Orser model, which consists of multiple springs that are coupled to dashpots in the place of the single spring in the Maxwell model. This model predicts a high frequency increase in *G*' as well as a minimum in *G*" at intermediate frequencies, as is seen in a variety of systems including Carbopol [36].

2.3 The Herschel-Bulkley Model

A model which describes the stress as a function of shear rate for a yield-stress fluid is the Herschel-Bulkey model shown below:

$$\sigma = \sigma_0 + k\dot{\gamma}^n. \tag{2.3.1}$$

The Herschel-Bulkley model is an empirical model developed to describe the behaviour of complex systems [37]. This model accounts for a yield stress σ_0 combined with power law behaviour in stress as a function of shear rate. The Herschel–Bulkley model predicts a viscosity that diverges continuously at low shear rates and is infinite below the yield stress [38]. The model reduces to the Bingham fluid model when n=1, where flow above the yield stress would be purely Newtonian and the constant k would represent the viscosity. Previous studies on Carbopol have shown that the Herschel-Bulkley model works well in describing the stress behaviour [27]. While the Herschel-Bulkley model works well in this regard, it is still an empirical model which has its limitations and lacks a sound theoretical underpinning [14,39].

2.4 The Effects of Jamming

Jamming is a phenomenon that occurs in particulate systems, whereby component particles become so closely packed that their motion becomes restricted. As the volume fraction of a system increases, the available space for particle motion decreases and system becomes jammed [40]. A jamming phase diagram can be drawn along the axes of pressure, as controlled by volume fraction, and shear stress; two distinct regimes, jammed and unjammed, are mapped out when yield stress is plotted as a function of pressure [41]. The jamming transition is accompanied by increases in the relaxation time and the length scale of local dynamical correlations in the system [41]. Jamming is also indicated by a non-zero value of the elastic modulus [40].

Jamming is frequently seen in deformable sphere systems, classic examples of which include emulsions and foams. An emulsion is a suspension of liquid drops in an immiscible fluid; a common example is oil beads in water. A foam is a suspension of gas bubbles in a liquid; common examples of foams include shaving cream and soap suds. Like microgel particles, the component particles in both of these systems will deform under the pressures of high volume fraction. In emulsions and foams it is the energetically unfavourable increase in the surface area of the droplets with deformation that gives the system its elasticity [42]. These systems differ from microgel and hard sphere systems in that they are more affected by aging, due to such factors as coalescence of bubbles and evaporation of the suspending fluid [43].

Jammed systems of compressible particles can reach quite high volume fractions, which approach unity. Consequently, volume fraction dependence of these systems is not

nearly as strong as it is for hard spheres [44]. Deformation in emulsions and microgels can be seen as analogous to temperature for molecular glasses in its effect on jamming; solid to liquid transitions in such systems can be driven by applied shears [45]. Once such a system enters a jammed state, thermal energy alone is unable to create rearrangements of particles, and the system will respond elastically to shear. Shear can cause further distortion in shape of the particles in a jammed system: whereas above the yield stress the particles respond to shear by hopping-type rearrangements in order to avoid significant deformation, below the yield stress the particles deform and absorb the stress elastically. The results of a comprehensive study of emulsion rheology performed by Mason *et al.* are summarized in the following paragraph [42].

The rheological behaviour of emulsions can range from purely viscous to elastic depending on volume fraction. In dilute emulsions, the viscoelastic moduli display hard-sphere-like behaviour. By contrast, in jammed emulsions, the viscous modulus displays a minimum as a function of frequency, while the elastic modulus displays a plateau. The minimum in the viscous modulus is thought to be due to a competition between particle rearrangements at low frequency and caged motion at high frequency. It is most pronounced at low volume fractions and gradually increases and flattens out at higher values. In most emulsions, the viscous modulus is significantly lower in magnitude than the elastic modulus. The plateau in the elastic modulus as a function of frequency is related to the capacity of the system for entropic energy storage; it is found to shrink down to an inflection point at low volume fractions. In jammed hard spheres the decrease in the elastic modulus at low frequencies is not present, while emulsion data

show this drop off even in the heavily jammed state; this is likely because the deformability of the particles allows for relaxations not present in hard spheres.

A critical mechanical energy appears to control the breakup and onset of the jammed state in a variety of diverse systems [45]. Sollich *et al.* have come up with a generic model for the rheology of soft glassy materials, which include foams, emulsions, and microgels, that they dub soft glassy rheology (SGR) [20,43,46]. This mean field model describes the trapping and caged dynamics that occur in such systems. The model defines an element of an intermediate length scale, which views an energetic landscape in which it can make hops to other configurations if given sufficient activation energy. The element deforms as it undergoes the rearrangement and then recovers in the new configuration. Such rearrangements alter the energy landscape, and thus, propagate more rearrangements. The model predicts Maxwell behaviour at low frequency followed by fairly constant viscoelastic moduli at intermediate frequency. The model also predicts the emergence of a yield stress at a set mean field noise temperature. One limitation of this model is that it applies only to the low frequency regime, where viscous effects are negligible, as it assumes that each element is purely elastic until rearrangement occurs.

3: PROPETIES OF MICROGEL SUSPENSIONS

3.1 Introduction

Microgels are systems that consist of swellable crosslinked polymer particles dispersed in a solution. Microgel systems display rheological behaviour that is a hybrid of sorts between that of polymer gels and that of hard sphere colloids. In order to fully understand the unique properties of these systems, it is useful to first consider the basic systems of linear polymers, polymer gels, and hard sphere colloids.

Chemical properties, such as crosslink density, and susceptibility to chemical or osmotic swelling, can affect the rheological behaviour and other physical properties of these systems in quite dramatic ways. In this chapter, we will provide a basic introduction to these chemical and physical properties, in order to provide a context for the observed behaviour of our Carbopol system.

3.2 Linear Polymers

A good starting point in the discussion of microgels is the simpler case of a linear polymer system. Linear polymers consist of free polymer chains dispersed in a solution with no permanent bonds or crosslinks between chains. In spite of its apparent simplicity, this system has many intriguing physical properties. Before discussing the behaviour of linear polymers, it is important to understand some basic concepts in polymer physics/chemistry such as overlap concentration, and entanglements.

An overlap concentration c^* is defined in order to distinguish between the cases of dilute and concentrated polymer dispersions. The overlap concentration is the critical concentration where the effective volumes occupied by the component polymer coils, as defined by the radii of gyration, begin to touch [47]. Below c^* the solution is dilute enough that polymer coils and their neighbors do not touch, and above c^* the coils are interpenetrating, and they share their respective volumes with neighboring coils [47]. This concept is illustrated in Figure 3.2.1. The overlap concentration is comparable with the localized concentration of a single polymer within its radius of gyration [48]. In the dilute limit, where $c<c^*$, the polymers behave essentially as hard spheres of radius R_g as the energy required for coils to overlap is quite costly [48]. In this limit the rheology of the system is governed by the dynamics and interactions of the coils with one another [48].

In the case of concentrated polymer systems, or polymer melts, some surprising behaviour is observed. One would suppose that the increased interactions between coils would complicate the picture, however, the physics governing chain morphology actually

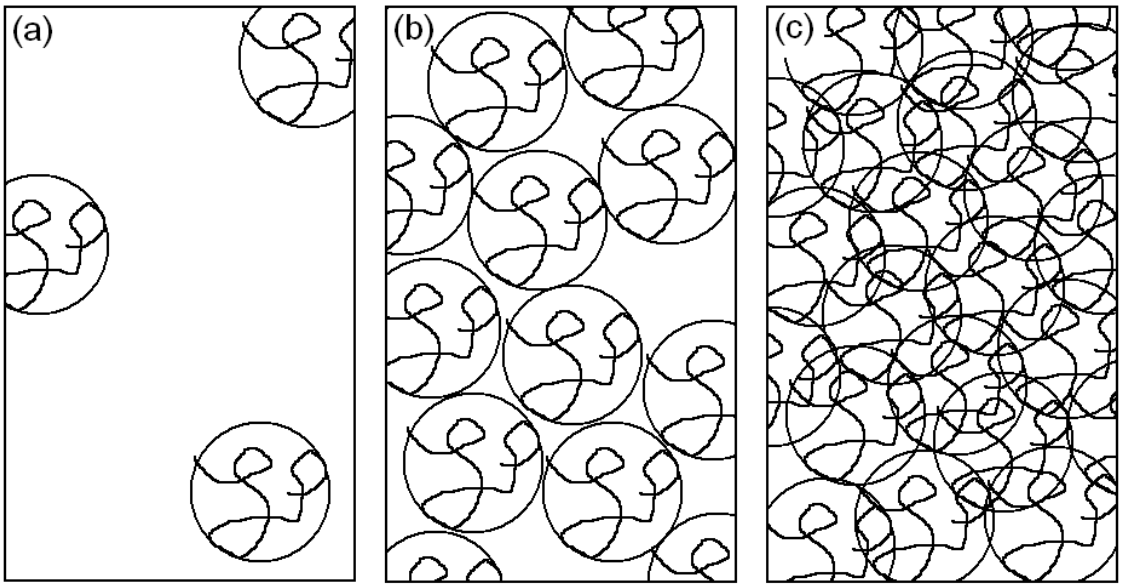

Figure 3.2.1: Illustration of overlap concentration, circles represent radius of gyration R_g: a) Dilute regime: $c<c^*$ b) Critical case: $c=c^*$ c) Concentrated regime: $c>c^*$.

becomes simpler: In contrast to the case in dilute systems, in a concentrated melt the mean square displacement between chain ends follows ideal Gaussian statistics [48]. In dilute polymers in good solvents, the excluded volume interaction and free energy of mixing lead the polymer coils to swell and occupy a greater space [48]. In the melt, by contrast, charge screening and excluded volume forces imposed by the other polymers act inwards and counteract the outward force that the polymer places on itself due to excluded volume interactions, and the individual chain within the melt is left in a homogeneous field [49]. This homogeneous field picture leads to a picture of the system where coils are fully interpenetrating and not simply overlapping, as previously thought [48]. This concept, which was pioneered by Flory [49], was controversial at its inception, yet in the decades since its predictions have been experimentally confirmed many times over [48].

The theory of reptation was introduced by de Gennes in 1971 to describe the motion of a single polymer chain around fixed obstacles [50]. This theory describes polymer chains as being confined to an effective tube created by neighbouring chains [51]. The only way the chain can move is via diffusion along the tube by sliding past the other coils [44]. If the chain is longer than the tube, the slack will allow for bends in the chain, or defects, which can travel down the tube like an "inchworm that is powered by Brownian motion" [51]. The motion of the chain can also over time modify the conformation of the tube [51]. Doi and Edwards later built on the theory using a mean field approach to tackle the motion of multiple interacting chains [51]. Although it is often evoked in discussions of the rheology of linear polymers, reptation still remains controversial, in whether it is applicable in situations of concentrated polymer melts, however the theory is widely accepted as applicable for dilute solutions[51,52].

Most polymers tend to be shear thinning, and show a decrease in viscosity with increasing shear rate. At high shear rates they are characterized by Newtonian behaviour, and display a constant viscosity [44]. Systems of hard spheres at the same molecular weight have been shown to flow more easily than linear polymers, this tells us that the hydrodynamic radius of the coils is an important variable [52]. In a high molecular weight polymer system, viscosity increases roughly linearly with concentration at low concentrations and then shows power law increases at higher concentrations [53]. This change in rate corresponds to the onset of overlap and entanglement [53].

Concentrated linear polymers form temporary entanglements, which are an analog of the crosslinks seen in gels [53]. Entanglements occur when polymer coils wrap around each other and restrict their range of motion; they are different than simple overlaps, and

result in a much stronger interaction [44]. In linear polymer systems, viscoelasitcity is dominated by these entanglements [31]. A plateau in the elastic modulus is seen in linear polymers when long chain lengths and high concentrations allow for the formation of entanglements [35]. The plateau of the elastic modulus has been found to vary as a power law with concentration in polystyrene [33]. Although these systems are capable of displaying elasticity, this does not imply that they possess a yield stress [46]: unlike the microgel systems to be discussed in later chapters, it has been shown that the viscosity of these systems does not diverge at low strain rates and that they do not posses yield stresses [31].

3.3 Polymer Gels

Polymer gels are systems of linear polymers which have been connected either physically or chemically [48]. Physical gels are formed in systems when there is an entropic preference for association between chains such as the formation of microcrystals between the segments of the polymer backbone as seen in block copolymers [48]. This type of gelation is most commonly seen in biological molecules, such as gelatin, and starches [48]. Most physical gels are weak gels; the component hydrogen bonds readily break under high temperatures and relatively weak stresses [48]. In a chemical gel, the covalent bonds are strong and unlikely to be broken by laboratory temperatures or rheological perturbations. In this chapter, we will mainly be concerning ourselves with chemical gels.

Chemical gels are formed by the creation of strong bonds between polymer chains, or crosslinks, which can be created by a few different types of chemical reactions: for example, they can be established by branch formation through a condensation reaction, or by the splitting of double bonds along a chain in a free radical reaction [48]. The conditions of the gel at formation can have a large impact on the its final form; factors such as whether the initial polymers were in dilute or semi-dilute suspension, whether they were polymerized in a good or a poor solvent, and the time over which the reaction took place, can all have significant effects [48]. With certain preparation methods it is possible to control the length of chains between crosslinks: chains of equal well-defined lengths can be prepared and the ends reacted with a polyfunctional unit to create crosslinks [48]. However in many gels this is not the case and crosslinks are found to be distributed inhomogeneously [54].

Chemical gels are created by starting from a sol or a liquid consisting of linear polymers and then adding crosslinking agents and initiating a reaction. As the amount of crosslinks is increased, larger and larger branched molecules are formed. When a certain critical number of crosslinks is reached, the entire network becomes connected by crosslinks and the system is considered a gel [48]. This critical point in the evolution of a crosslinked system is known as the gel point. The gel point can be measured as the crosslink concentration where the elastic and viscous moduli of the system G' and G'' become roughly equal in magnitude [55].

In a system which has crosslinks, as opposed to only entanglements, mechanical deformations become reversible [56]. The crosslinks keep the strands of the polymer chains from displacing very far from their initial positions during a disturbance and

prevent the flow of polymer strands relative to each other, thus the material is able to recover its original structure [35]. By contrast, linear polymers are only able to recover from short deformations, as longer deformations lead to an irreversible change in conformation in the material [35].

The restoring force in crosslinked systems is due to the entropic cost of the change in conformation of the polymer chain [35]. An additional contribution to the elasticity in gels comes from topological constraints on the configuration of the chain segments between crosslinks [51]. The elastic modulus G can be calculated from the temperature T, density ρ, and the average molecular weight between crosslinks M_x, where R is the gas constant [35]:

$$G = \frac{\rho RT}{M_x}. \tag{3.3.1}$$

The elastic modulus can also be written in terms of the crosslink density n where k_B is Boltzmann's constant:

$$G = nk_BT. \tag{3.3.2}$$

In many systems, the elastic modulus may in fact be larger than the values obtained from the above equations due to contributions from entanglements between chains in addition to crosslinks [35].

3.4 Hard Sphere Colloids

Hard sphere colloids are systems of Brownian-scale particles where the excluded volume interaction is the only potential present [18]. Hard sphere systems undergo a transition from liquid to glass at a well known volume fraction φ of 0.49, and they further achieve maximum random close packing at φ=0.64 [18]. In the glass state, the particles form cages, which trap each other and restrict motion. When low frequency small oscillatory shears are applied to such a system, the system is able to relax through the Brownian motion of the component particles. At higher frequencies, the system has no time to relax to accommodate the perturbations and must store elastic energy [18]. As φ is increased both the suspension relaxation time and the elastic modulus increase as well [34,53].

Hard sphere systems tend to be weakly elastic, which results from energy stored due to changes from equilibrium configuration with applied shear this elasticity is dampened somewhat by the tendency to relax through Brownian motion, however, they still possess a finite plateau in $G'(\omega)$ [53]. At low φ the system is primarily viscous with a constant G''/ω, which is higher than G' [18]. When an attractive interaction is added to the hard sphere potential the system becomes highly elastic with $G' \gg G''$ [53].

Hard spheres have been found to display a yield stress at high volume fractions [53]. Hard spheres are thixotropic, which means that they display long-timescale structural relaxation [53]. Thixotropy is detected by the presence of hysteresis in a flow curve, or plot of stress versus shear rate [53]. Hard sphere systems also display shear

thinning at higher shear rates, when Brownian motion is not sufficient to relax the system and particles flow and rearrange themselves irreversibly [57].

For hard spheres, the viscosity can be predicted by the Batchelor equation below [53]:

$$\eta = \eta_0(1 + 2.5\varphi + 6.2\varphi^2), \tag{3.4.1}$$

where η_0 is the zero-shear, or intrinsic, viscosity. Intrinsic viscosity can be obtained from the intercept of a viscosity as a function of shear-rate curve, and can also be obtained from the viscous moduli as a function of frequency as follows [33]:

$$\eta_0 = \lim_{\omega \to 0} \frac{G''(\omega)}{\omega}. \tag{3.4.2}$$

The first finite-volume fraction correction term of Equation 3.4.1 was calculated by Einstein for the case of viscous dissipation produced by flow around a sphere [53]. In its original form the equation only applies in the dilute case where flow around a given sphere is unhindered by the presence of neighboring spheres. Later, Batchelor modified the formula to account for two-body interactions by calculating an second order term [53]. This equation proves useful in cases where viscosity data is easily obtainable and volume fraction is unknown.

3.5 Microgels

Microgels are large molecules of colloid scale, which are composed of a crosslinked network of polymers [54]. They were first synthesized in 1935 from divinylbenzene by Staudinger and Husemann [54]. Since then, microgels have been synthesized from a variety of different polymers and crosslinkers and dispersed in a variety of solutions from organic to aqueous. Microgels are useful for a variety of practical applications, from use in industrial grade lubricants to drug delivery systems. Their usefulness is due, in great part, to their unique rheological properties. Microgel particles have the compressibility of foams and emulsions, they display jamming analogous to hard spheres, yet they still retain much of the behaviour and chemistry of their composite polymer chains. This makes them an intriguing rheological case to study. In this chapter we will consider several properties of microgels. According to Cloitre, there are three basic forces at play which effect microgel rheology: elastic restoring forces created by crosslinks, frictional forces created by dangling ends, and stochastic forces resulting from ion imbalances [21].

Crosslink density has a large effect on the rheological behaviour of microgels. The degree of crosslinking within the particles maps out a spectrum of behaviour ranging from that of linear polymers with no crosslinks, to branched and star polymers with few crosslinks, to conventional microgels to with an intermediate number, all the way to densely crosslinked and highly elastic hard sphere colloids [58]. Some microgel particles are thought to have a crosslinked core surrounded by a shell of dangling polymer chains [59]. The higher the degree of crosslinking, the more elastic the particles are as

suggested by Equation 3.3.2. A greater degree of crosslinking is also found to increase the viscosity of a microgel suspension, as found early on by Taylor and Bagley [23, 24]. When particles have a higher crosslink density, they have fewer dangling ends on their surfaces, and hence they experience less entanglement with neighbouring particles; this leads them to behave less like linear polymers and more like hard spheres [21]. Correspondingly, the lower the crosslink density, the softer the microgels are, and the more pronounced their dangling tails become, which leads to a greater degree of inter-particle interaction [60].

Due to their lower elasticity, microgel particles, unlike hard spheres, are quite compressible and a conventional measure of volume fraction will not suit them beyond the dilute regime [61]. It has been shown that soft particles are not fully jammed at the known random close packing limit of hard spheres [61]. Deviations from hard sphere behaviour are more pronounced in microgels at higher concentrations, where the compressibility of the particles begins to play a greater role [60]. Further, it is possible for a concentrated microgel suspension to fill the entire space, whereby φ=1. Compaction in concentrated microgels creates a paste where particles have large flattened areas of contact or facets that lead to significant particle interlocking and steric interactions between loose ends [11,62]. It has also been found that the ratio of radius of gyration R_g to the hydrodynamic radius R_H is significantly smaller than the value seen for homogeneous spheres [59]. This nonuniformity is thought to be attributed to the loose chains extending from the surface of the microgel particles [59]. These loose ends contribute little to the overall mass of the particles, and correspondingly R_g, but they have significant effects on hydrodynamics and R_H [59]. Similarly, it has also been shown that

when a steric polymer layer is added to hard sphere colloids, the particles' behaviour begins to deviate substantially from that of hard spheres [60].

The rheological behaviour of microgel suspensions depends greatly on the chemistry of the component polymers, which determines their susceptibility to osmotic swelling. A polyelectrolyte is a type of polymer that is particularly prone to swelling due to the presence of ionizable groups. These groups can dissociate in an aqueous solution into a fixed ion, which sits on the polymer backbone, and a mobile counter ion [63]. In polyelectrolyte systems, osmotic pressure plays a much bigger role than in unionizable systems [63]. In a polyelectrolyte microgel, the concentration of free ions is higher within the microgel particles than in the surrounding fluid [49]. The electrostatic attraction to the counter ions keeps the vast majority of mobile ions trapped within the gel in order to keep the particles electrically neutral [31]. This creates an effective membrane, which keeps the majority of the mobile ions within the particles and prevents diffusion into the solution [49]. This is analogous to the case of Donnan equilibrium: free ions must find an equilibrium state between osmotically driven diffusion into the surrounding less concentrated aqueous solution and electrostatic attraction to the positive charge within the particles, which is created by the fixed counter ions [26]. Donnan theory attributes the swelling of ionic gels to this imbalance in osmotic pressure between the ions in the gel and the outer solution [64]. Swelling occurs as water is drawn into the particles to dilute the concentration of ions and to increase its free energy. A schematic diagram illustrating this concept is shown in Figure 3.5.1.

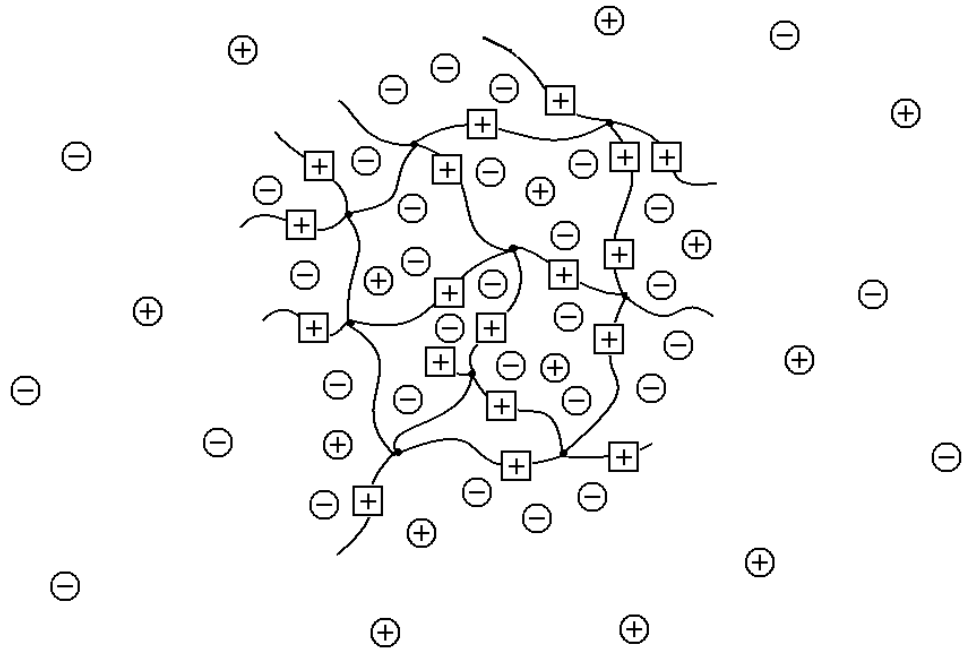

Figure 3.5.1: Illustration of Donnan Equilibrium: charges in squares represent fixed charge groups while those in circles represent mobile ions, which are free to be exchanged with the surrounding solution.

In a polyelectrolyte microgel, the chemical environment of the surrounding fluid controls ionic swelling and changes to it can significantly alter particle size and overall gel behaviour [31]. The microgels will not swell until ions are added, as in the pH-unmodified state they are not soluble in water. This is evidenced by the milky white appearance an pH-unmodified polyelectrolyte microgel dispersion takes and the subsequent increase in clarity upon titration with NaOH [31]. At maximum swelling, there is a balance of osmotic pressure inside and outside of the gel particles: the elastic pressure of the gel due to the crosslinks along with the osmotic pressure created by the trapped ions leads to an inward pressure, which is balanced by an outward osmotic pressure created by the free ions added to the solution [31]. Higher crosslinked systems

do not swell as much as those of lower crosslinking due to the increased contribution of inward elastic pressure [65]. Osmotic effects have also been shown to lead to particle shrinkage in microgels at high volume fraction and pH when there is a surplus of free ions outside of the particles [31].

Swelling decreases component particle elasticity, but it increases overall system volume fraction, which affects viscosity, elasticity, and yield stress [34]. Since microgels cannot interpenetrate each other as much as linear polymers can, they become compressed at high volume fraction, which results in a viscosity that increases more rapidly with concentration above c^*; the higher the crosslink density is the more dramatic this effect will be [29]. The compressibility of microgels makes them unique in their rheological behaviour from the previously discussed systems. Compressibility allows for increased elasticity as well as decreased rigidity, or ability to avoid structural collapse under shear; unlike the more rigid structures formed by hard spheres, microgel structures are less prone to 'snap' under high shear, as they can deform significantly without compromising their configurations. This gives microgels both a high elasticity and yield-stress behaviour that shows little evidence of thixotropic effects.

3.6 Carbopol Gels

Carbopol microgels, also known as carbomers, carboxyvinyl polymers, and carboxy polymethylene, are a family of microgels that are composed of linear poly(acrylic acid) crosslinked with allyl sucrose [8]. Carbopol was originally developed

as an industrial thickening agent by the laboratories of BF Goodrich for use in tires [8]. Today, its rights are owned by pharmaceutical companies, who use it in a variety of drug delivery methods. The significant yield stress of Carbopol even at very low concentrations allows for the entrapment of drugs within its structure, which makes it very useful for slow release applications. Carbopol is also used in a variety of other commercial and industrial applications. For example, Carbopol microgels are used to stabilize detergents, to prevent the sedimentation of abrasives in scouring products, and to reduce splashing in bleaches [66].

Carbopol is prepared by inverse emulsion polymerization in organic solvent [67]. Conventional emulsion polymerization is performed by combining an aqueous medium with small amounts of an emulsifier, a water soluble initiator, and monomers [49]. In inverse emulsion polymerization the ratio of oil to aqueous solution is reversed [68]. These techniques are more rapid than bulk single phase polymerization methods, and allow for higher molecular weights to be obtained [68]. In conventional emulsion polymerization, an emulsion of micelles is formed by the emulsifier. Polymerization occurs in two stages: In the initial stage, the growth of the polymers occurs in dispersed phase, as micelle aggregates stabilize the monomer droplets and polymerization begins to take place. Later on, as polymerization progresses, the polymer chains expand beyond the radius of the micelles, and polymerization continues at slower rate in the surrounding continuous medium [49]. The now predominantly polymer particles continue to grow and gain monomers. At this stage, new smaller particles do not readily form due to high surface tension costs [49]. The two distinct polymerization rates of emulsion polymerization lead to two different regimes within the microgel particles: a dense core

created by the rapid polymerization of the initial stage, and a loose shell from the slower rate of the final stage [54]. This gives the particles a characteristic non-uniform crosslink density, where crosslinking is strongest at the center and lowest at the periphery.

In its simplest form, Carbopol is a dry polymer powder which swells upon dispersion in an aqueous solution. Due to its crosslinks, Carbopol is not soluble in aqueous solutions. It is mildly acidic with an acid dissociation constant, pK_a, that has been measured at around 6.7 to 7 [69]. This is higher than that of linear (poly)acrylic acid, which has a pK_a of 5.3, and that of monomers of acrylic acid, which have a pK_a of 4.3 [69]. The difference between the monomer and polymer values is related to the splitting of a double bond with polymerization, which modifies the electronegativity of the carboxylic groups. When salts are added the pK_a is lowered closer to the monomer value due to charge screening [69].

The backbone of (poly)acrylic acid posses a carboxyl (COOH) group, which dissociates in aqueous solution, thus it is a polyelectrolyte. The chemical structure of (poly)acrylic acid is shown in Figure 3.6.1. The carboxyl groups serve as the fixed anions and protons as the mobile cations. As in other polyelectrolytes, osmotic effects play a strong role in the swelling behaviour of Carbopol [31,62]. Swelling is caused by an increase in solubility with increasing pH and electrostatic repulsion between chains [59]. Upon titration with a basic solution, the carboxyl groups ionize and mutual ionic repulsion leads to the expansion of the microgel particles [26]. Carbopol is very sensitive to even the slightest changes in pH or ionic strength. The effects can be observed in both its bulk and microscopic properties. Light scattering experiments done on similar microgels composed of crosslinked ethyl acrylate show that upon titration with NaOH

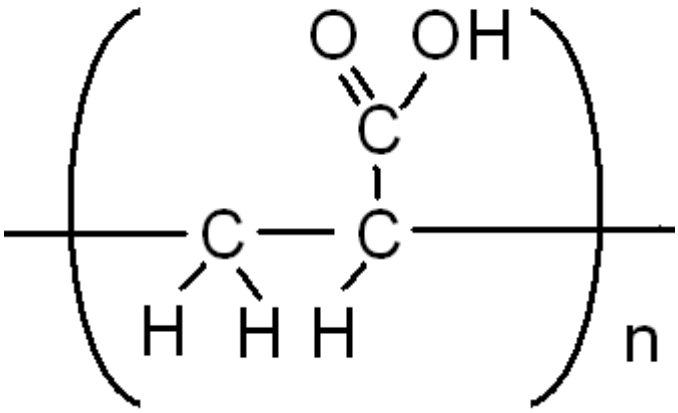

Figure 3.6.1: The chemical structure of (poly)acrylic acid.

particles swell by up to 200 times in volume [59]. It has also been observed that the addition of an inert electrolyte leads to deswelling due to screening of the positive groups [54].

Carbopol is a molecule that has a very high molecular weight, which is estimated to be on the order of 100 M Dalton [70]. Carbopol molecules form micron-scale sponges that aggregate and jam. At low concentrations, Carbopol gels display near-Newtonian behaviour [32]. In this regime, Carbopol's behaviour resembles that of dilute hard spheres [11]. The divergence of the zero-shear viscosity and the appearance of a yield stress are observed at critical concentrations [71]. The onset of this behaviour occurs at quite low concentrations approximately around 0.5 wt%, depending on the variety of Carbopol.

Carbopol gels show little to no thixotropic behaviour [26,32,70]. Small traces of hysteresis are seen at low concentrations of pH-unmodified Carbopols, where the particles are more tightly bound and hard sphere-like [70,72]. Creep, or long-timescale

structural relaxation has been seen in Carbopol; however, it appears to occur only at very long timescales, which are on the order of weeks to months [73].

Microrheological techniques, such as particle tracking with fluorescence microscopy, have yielded valuable information about the structure of microgels [25,74]. This technique employs three-dimensional microscope imaging and particle tracking analysis to examine the dynamics of small probe, or tracer, particles within the microgel. Microrheological results are found to show good agreement with the bulk rheology, when the tracer particles used are large compared to the length scales of the underlying structure [75,76]. A microrheological study of Carbopol by Oopong and de Bruyn has shown the existence of two different dynamical populations of tracer particles: slow particles that correspond to the particles trapped within microgel particles, and fast particles that probe the surrounding fluid [71,74]. The tracer particle dynamics allow two phases to be mapped out: slow particles map out the solid (swollen particle) phase, and fast particles the liquid (solvent) phase. With increases in concentration, the volume fraction of the solid phase was found to increase at the expense of that of the liquid phase [71]. At low concentrations, the particles are swollen and non-interacting and there are two clearly separated phases of polymer and solvent [77]. Structures formed at intermediate concentrations were found to be percolated networks of microgel particles with dispersed solvent ponds [71]. In Figure 3.6.2, a conceptual illustration of this type of structure is shown.

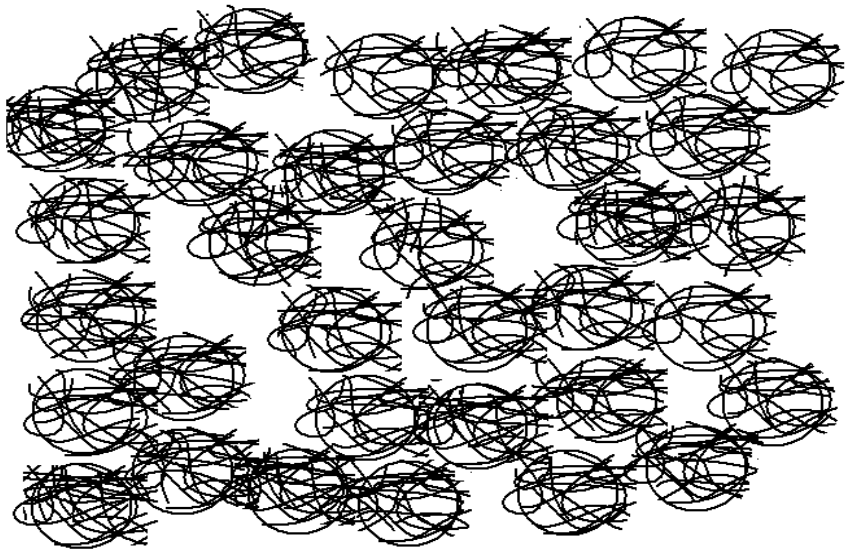

Figure 3.6.2: Conceptual illustration of the proposed meso-scale structure of a Carbopol gel. Note the voids amongst the aggregated spongy particles.

At intermediate concentrations, there is interplay between volume fraction and component particle hardness, which affects rheological properties [77]. At higher volume fractions, above the overlap concentration c^*, the particles become compressed and form a stable homogeneous structure. Such structures consist of a paste of compressed particles, which are able to fill much of the interstitial space. An illustration of this type of structure is shown in Figure 3.6.3.

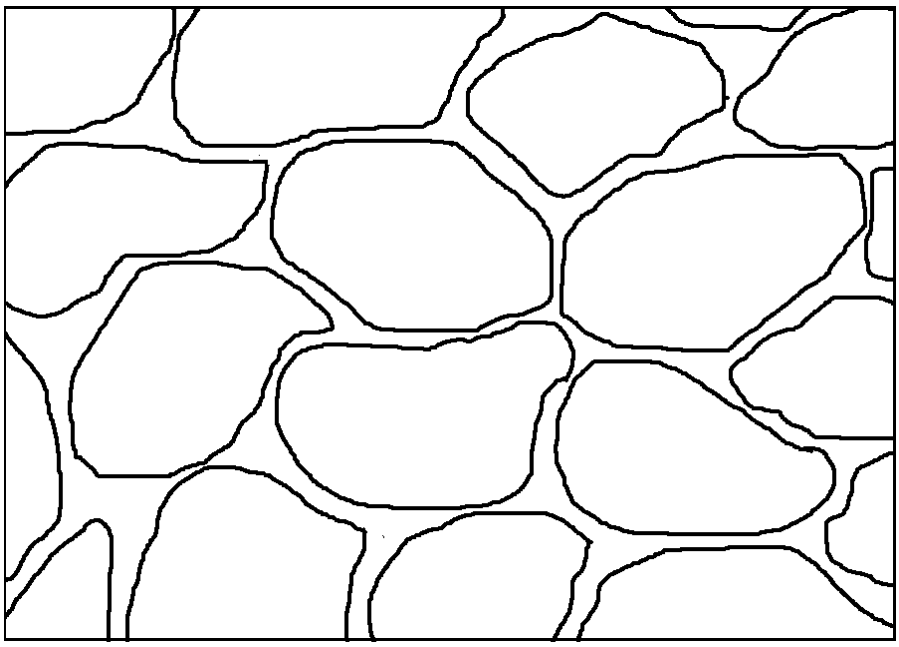

Figure 3.6.3: Illustration of a paste of compressed particles.

In the previously mentioned microheology study it was found that as concentration is increased further, all of the tracer particles become trapped by the microgel particles [71]. This indicates that the system is effectively an elastic network [71]. This coexistence behaviour along the route to gelation can be viewed as analogous to a 1^{st} order phase transition [71].

4: EXPERIMENTAL METHODS

4.1 Introduction

This chapter details the experimental procedures involved in obtaining the results of the following chapter. In Section 4.2, we discuss the preparation of Carbopol samples. Then in Section 4.3, we introduce the geometry of the cone and plate rheometer, and in Section 4.4, we discuss the taking of rheological measurements.

The next two sections, 4.5 and 4.6, detail the experimental procedures and results obtained from some supplementary measurements done with optical microscopy and light scattering performed on the Carbopol samples. We employed these techniques in an effort to obtain some information about the underlying microstructure of the Carbopol samples. We performed optical microscopy on samples of Carbopol ETD 2050 to obtain some rough estimates of particle size in the pH-unmodified samples. An extensive study of light scattering on Carbol ETD 2050 was performed by a previous graduate student of the Frisken lab, David Lee, and the results are detailed in his MSc thesis [78]. We

performed a much less extensive follow up study on the samples of Carbopol Ultrez 10 to give some basic information about the fractal dimensions of the samples.

4.2 Sample Preparation

For our experiments we chose Carbopol varieties ETD 2050 and Ultrez10. There are several different varieties of Carbopol, which are made with slightly different preparation methods. Changes in preparation methods can lead to subtle differences in performance: crosslinker type, solvent and drying temperatures, and time of polymerization have all been shown to have effects [66]. Early studies of Carbopol mainly centered around the 940 and 941 varieties [15,23,26,27,29,65,70], of which ETD 2050 and Ultrez 10 are the current faster wetting, easier to disperse analogs [8]. The ETD and Ultrez series of Carbopols are easier to hydrate, less prone to forming lumps, and less viscous in the pH-unmodified state, all of which allow for easier and more consistent sample preparation [8,32,77].

Carbopols 941 and ETD 2050, which have lower crosslink densities than Carbopols 940 and Ultrez 10, open up and fill space easily at low concentrations, which makes them more viscous at low concentrations and pH compared to Carbopols 940 and Ultrez 10, which have more compact particles and larger interstitial spaces at low concentrations [8]. The situation is quickly reversed after titration with NaOH, when the more rigid structures formed by the higher crosslinked Carbopols give higher viscosity and elasticity.

In order to create the initial gel, powders of Carbopols ETD 2050 and Ultrez 10, obtained from Noveon Pharmaceuticals, were slowly dispersed in deionized Millipore filtered water. This was done by creating a gentle vortex in a 500mL beaker with a large magnetic stir bar over a stir plate. Powder was added in small increments to the centre of the vortex. Concentrations were determined by percent weight by volume and the dry Carbopol was carefully weighed in an electronic balance prior to being added. The mixture was allowed to stir for several days, in order to ensure that the Carbopol was fully hydrated. Afterwards the original batch was portioned out and diluted accordingly with deionized Millipore water to obtain a range of concentrations. The concentrations were chosen based on the predicted viscosities of the resulting dispersions to ensure that they could be adequately mixed within the lab with the stir plate setup, as we did not have access to industrial mixers. For Carbopol ETD 2050, we chose to make concentrations of 0.1, 0.2, 0.5, 1, 1.5, and 2 wt%. All values of wt% quoted in this thesis were taken from weight percent by volume. A single pH-unmodified sample at a concentration of 5.0 wt% was also prepared and analyzed. However, a range of pH values was not prepared at this concentration due to its extremely high viscosity, which was prohibitive to the homogenous dispersion of ions, needed to obtain a constant pH throughout the sample. For the significantly more viscous Carbopol Ultrez 10, we chose concentrations of 0.05, 0.1, 0.2, and 0.5 wt%.

After we ensured that the polymers were sufficiently hydrated, as confirmed by the absence of visible conglomerates, we began the titration with NaOH of the samples to obtain a range of pH. We used a 20 wt% NaOH solution to titrate the samples. Small amounts of NaOH were added with a pipette and then the samples were gently agitated

with a vortexer and allowed to equilibrate. We found that it took a fairly long time, on the order of several hours, for the pH of the samples to stabilize. We believe that this was due to dramatic localized increases in viscosity with the addition of droplets of NaOH solution to the gel. We also found that we needed to leave the digital pH probe in the gel for a relatively long time of around 20 minutes or more to allow the reading to stabilize. For each sample we obtained a range of pH from that of the pH-unmodified sample, which was approximately pH 2.5 to 3.5 depending on the concentration, to pH 11 for each concentration. The pH meter essentially measures the chemical potential of H^+ which at equilibrium is the same within the gel as it is with the outer solution [64]. During the base titration process we were careful not to overshoot pH, and we did not add any acid for corrections, as this would lead to charge screening, which can have quite dramatic effects on the sample's viscosity [29]. After all pH values had been measured, we then centrifuged the samples at a rate of 1,000 RPM to rid them of small bubbles which could affect the rheology.

4.3 The Cone and Plate Rheometer

A cone and plate rheometer is an ideal apparatus for the study of both the static and dynamic properties of a viscoelastic fluid. Its symmetrical geometry gives a shear rate that is independent of cone radius. A cone and plate rheometer is also an ideal because it requires a relatively low sample volume, and is easy to clean. MRI velocimetry of

Carbopol has shown that cone and plate bulk rheometry gives an accurate picture of steady shear flow [79]. A simple diagram of the geometry is shown in Figure 4.3.1.

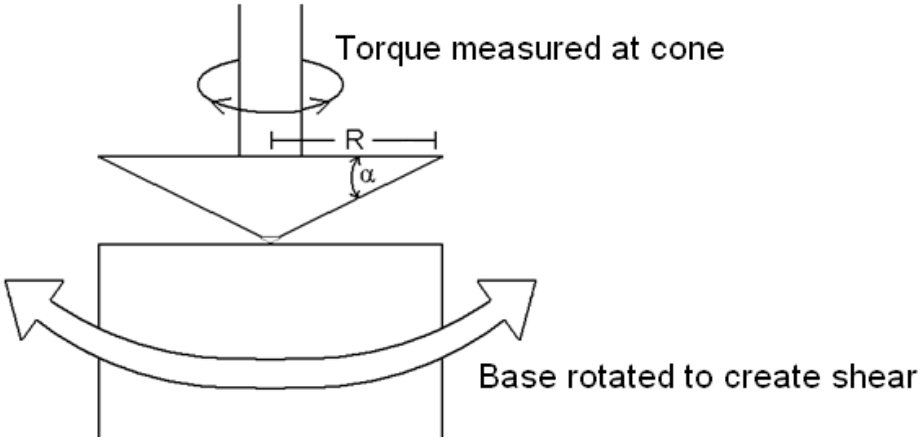

Figure 4.3.1: Illustration of the schematics of the cone and plate rheometer. α is the cone angle and *R* is the radius of the base of the cone.

The simplest way to study the stress response of a fluid system is to apply a steady shear to the bottom of a sample and measure the stress on the top. For a cone and plate setup where α is the cone angle in radians, the shear rate for a given angular rotation speed Ω is given by

$$\dot{\gamma} = \frac{\Omega}{\tan \alpha}. \tag{4.3.1}$$

The shear applied at the plate to the bottom of the sample will induce a torque *N* on the cone at the top of the sample. Torque is measured at the top of the cone with a digital force balance transducer, which contains a feedback circuit that measures the torque on the transducer, then amplifies the resulting voltage signal and uses it to keep the torque transducer fixed in angular position.From this torque response the shear stress σ can be calculated, as

$$\sigma = \frac{3N}{2\pi R^3}, \tag{4.3.2}$$

where *R* is the radius of the plate. With the shear stress known, the viscosity can be found by simply dividing the shear stress by the shear rate:

$$\eta = \frac{3N\alpha}{2\pi R^3 \Omega}. \tag{4.3.3}$$

A cone and plate rheometer can also be used to make small amplitude oscillatory shear measurements (SAOS). An oscillating angular frequency is simply applied at the base and then the in-phase and out-of phase components of the torque response are measured at the cone. For an applied driving oscillation of the form

$$\Omega(t) = \Omega_0 \cos(\omega t), \tag{4.3.4}$$

a shear rate, of the form shown below, will be induced

$$\dot{\gamma}(t) = \frac{\Omega_0 \cos(\omega t)}{\tan(\alpha)}. \tag{4.3.5}$$

Since strain is simply the time integral of the shear rate,

$$\gamma(t) = \int_0^t \dot{\gamma}(\tilde{t}) d\tilde{t} \tag{4.3.6}$$

by substituting Equation 4.3.4 into Equation 4.3.6 we can easily obtain the oscillatory form of the strain,

$$\gamma(t) = \frac{\Omega_0}{\omega \tan(\alpha)} \sin(\omega t) = \gamma_0 \sin(\omega t), \tag{4.3.7}$$

where the strain amplitude γ_0 is given by

$$\gamma_0 \equiv \frac{\Omega_0}{\omega \tan(\alpha)}. \tag{4.3.8}$$

From this applied strain an oscillatory stress response is observed in the form

$$\sigma(t) = \gamma_0 \left(G'(\omega)\sin(\omega t) + G''(\omega)\cos(\omega t) \right), \tag{4.3.9}$$

where the magnitudes of the in-phase and out-of-phase components of the response *G*' and *G*" are known as the elastic and viscous moduli, respectively. They can be defined more explicitly, with

$$G'(\omega) = \frac{\sigma_0}{\gamma_0}\cos\delta, \tag{4.3.10}$$

and

$$G''(\omega) = \frac{\sigma_0}{\gamma_0}\sin\delta, \tag{4.3.11}$$

where δ is the phase angle, whose tangent is commonly known as the loss tangent,

$$\tan\delta \equiv \frac{G''}{G'}. \tag{4.3.12}$$

The measurement of the above quantities allows us to obtain a broad picture of the rheology of a sample across several different regimes.

4.4 Rheometry Setup

All rheometry was performed in the laboratory of Prof. John de Bruyn at the University of Western Ontario using an Ares RHS strain-controlled rheometer that was outfitted with a standard cone and plate setup. Slip is a cause of concern and can distort the flow curves and hinder accurate measurements of yield stress and viscosity,

especially in highly viscous samples [12]. Sandpaper was attached to both the plate and edge of the cone with epoxy to prevent slip. The paper was carefully applied to ensure that there were no significant bumps which might affect the rheology. Although there was no sandpaper applied at the center of the cone, the contributions to the stress from this region are significantly smaller from those at the outer edge, as the shear stress is proportional to the radius cubed. The gap between cone and plate was adjusted accordingly to account for the change in separation between the surfaces due to the sandpaper thickness.

Before performing tests we checked the pressure gauges on the rheometer to make sure they were at 35 and 60 psi to ensure optimal function of the transducers. This is done because the rheometer has an air bearing which allows for a greater sensitivity [34]. We employed a water bath connected to the rheometer to keep the samples at a constant 25°C. The cone used was 5 cm in diameter and had an angle of 0.04 radians. For each set of tests, we added approximately 1.5 mL of sample to the center of the plate. The cone was slowly and carefully lowered down by a motor controlled through the computer interface, until the proper gap height of 0.04 cm was reached. We then waited for several minutes for the normal force at the cone, as measured by the transducer, to dissipate. We used a small spatula to scrape off the excess sample which had seeped beyond the edge of the plate, in order to obtain a clean edge of sample between cone and plate. We fitted the rheometer with a humidity cover saturated with water to prevent sample evaporation. The transducer on the rheometer has two settings with different sensitivities. It is important to start each test in rough setting, to prevent damage to the transducer, and then

switch over to the finer setting when necessary to obtain more accurate measurements. This switch was automatically made by the software during measurements.

Three standard tests were performed on each sample. Oscillatory tests were performed first, as steady state shear rate sweeping tests have the potential to destroy microstructure. During oscillatory tests, the base of the rheometer is driven with an oscillating angular frequency and the stress response is measured through a transducer attached to the cone. Before each test, a pre-shear at a frequency of 1rad/s was applied to the sample for 30 seconds, in order to clear previous history. For the initial oscillatory measurement, we varied the strain amplitude applied to the sample while keeping the driving frequency constant at 1rad/s in order to measure the viscous and elastic moduli as a function of percent strain. In a second test, we measured the viscoelastic moduli as functions of frequency. This test needs to be performed in the linear response regime so we can be assured that it is not destructive to the microstructure [27]. We kept a constant amplitude of 1% strain, while varying the driving frequency from 0.05 to 300 rad/s. For both types of oscillatory measurements we obtained the viscous and elastic moduli from the in-phase and out-of-phase components of oscillation observed on the cone.

For a third test, we used the rheometer in steady state mode and measured viscosity and stress as a function of shear rate. In this mode, the base or plate of the rheometer rotates for a period of time at a fixed angular velocity and shear rate, while the resulting stress on the cone is measured from the normal force read at the transducer. This measurement yields a flow curve, or plot of stress and viscosity as functions of shear rate.

4.5 Optical Microscopy

We took and analyzed several optical microscope images of hydrated Carbopol ETD 2050 samples. We placed a small amount of the Carbopol dispersion on a glass slide and then covered it with a cover slip. A Ph3 phase contrast filter was used with a bright field Olympus BX51 microscope. Images were taken at a range of magnifications from 10X to 100X . Images taken at 100x were taken with an oil immersion lens. Digital images were taken with a Roper Scientific Photometrics CoolSNAPcf camera and later analyzed in Matlab for evidence of intensity correlations using a simple linear correlation function.

The use of a phase contrast filter allowed for differences in local density to be seen. The higher density regions appear lighter than those of lower density. Beyond even the slightest amount of titration with NaOH, the contrast observed in the samples began to disappear. Thus, the only images suitable for analysis were those of the pH-unmodified samples. An image of an pH-unmodified sample of Carbopol ETD 2050 is shown in Figure 4.5.1. Note the appearance of light and dark regions scattered across the image.

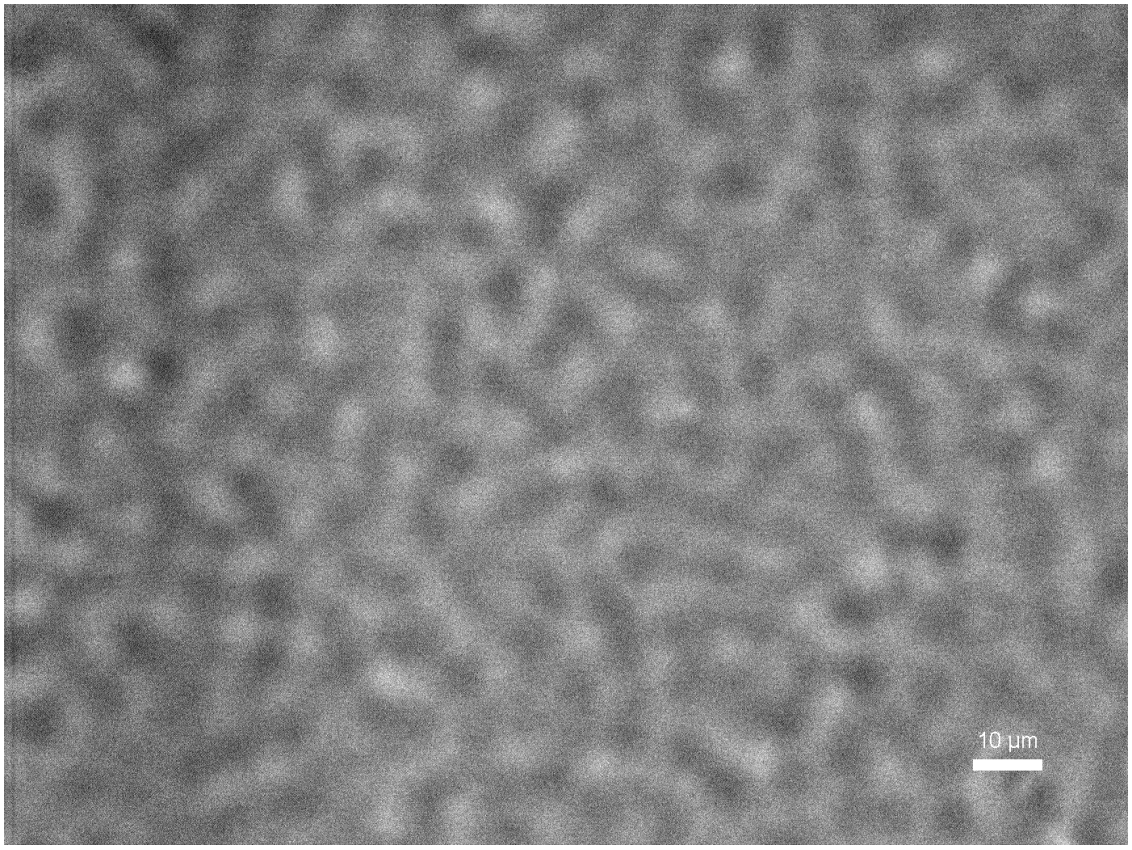

Figure 4.5.1: Image taken of 2wt% pH-unmodified hydrated Carbopol ETD 2050 sample at 40x magnification with a ph3 phase contrast filter.

We coded a correlation function in Matlab in order to analyze the correlations in the above image. The algorithm calculated the correlation in intensities between neighbouring pixels. The formula for the correlation function $G(r)$ is given below, where $I(r)$ is the intensity at a point r:

$$G(r) = \frac{\langle I(r') \cdot I(r'+r) \rangle}{\langle I(r') \rangle^2}. \qquad (4.5.1)$$

A plot of this correlation function is shown in Figure 4.5.2.

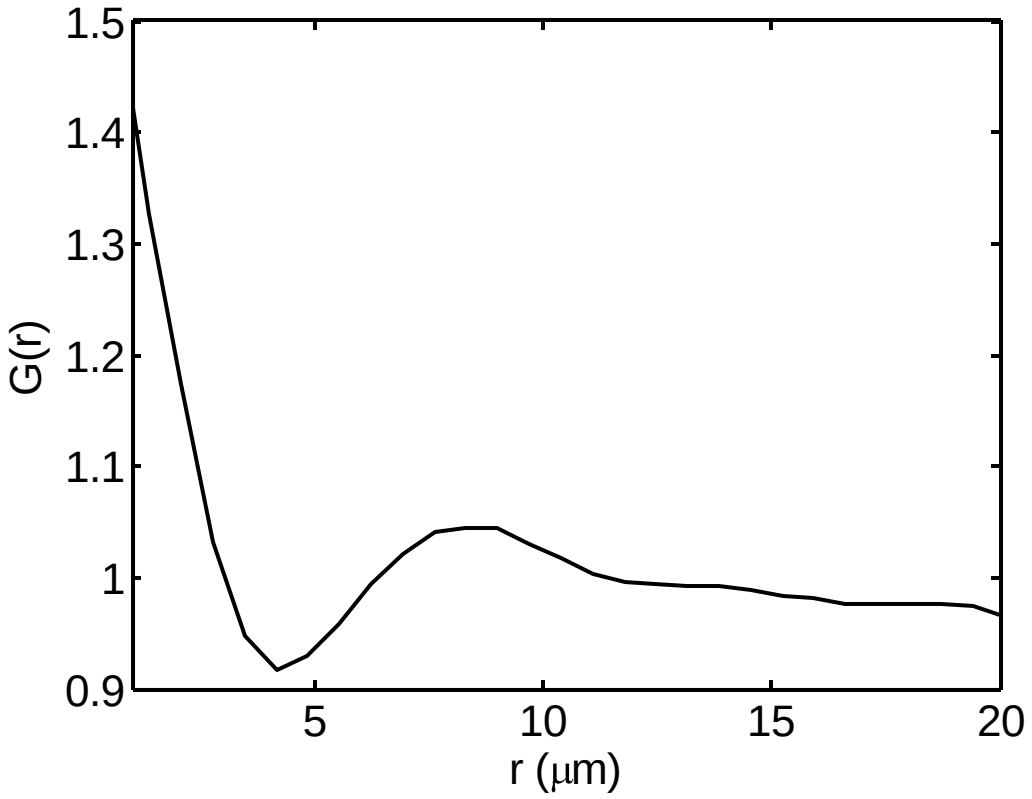

Figure 4.5.2: Intensity correlation function of image in Figure 4.5.1.

Note the appearance of two clear peaks in the plot of Figure 4.5.2, the first centred at the origin corresponds to intraparticle correlations and the second centred around 8 microns corresponds to nearest neighbour correlations between particles. The separation between these peaks is related to the average separation between a particle and its nearest neighbour. This gives us an estimate of about 4 microns for the radius of an unmodified particle. This result is in rough agreement with results obtained using small angle light scattering which gave the radius of a pH-unmodified particle as between 6-24 μm [28,78].

4.6 Light Scattering

Light scattering allows for information about particle sizes to be gathered from the light scattered by a sample at a range of angles. An incident beam is directed at the sample and the scattered intensity in the same plane is measured across a range of angles. The geometry of a light scattering apparatus is illustrated in Figure 4.6.1.

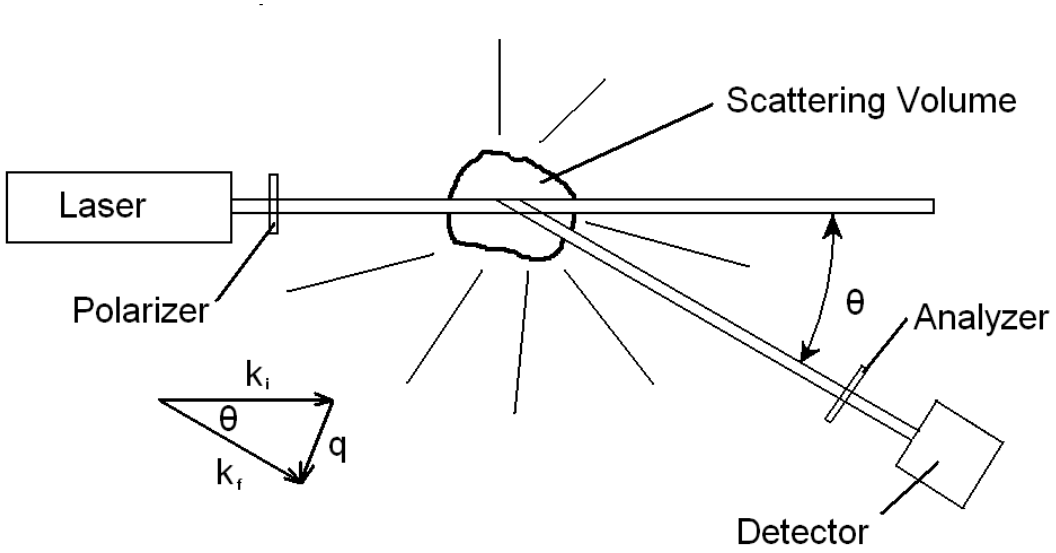

Figure 4.6.1: Schematic diagram of a light scattering apparatus.

In the figure we see an initial wavevector k_i is scattered by an angle θ, and a final wavevector k_f is measured at the detector. The scattering vector q is given by the vector difference. If the wavelength λ is not altered by the scattering process the wavevector is given by [80]:

$$q = \frac{4\pi n}{\lambda} \sin\left(\frac{\theta}{2}\right). \tag{4.6.1}$$

For a linearly polarized incident beam the intensity of scattered light is given by [80]:

$$I_s = \frac{16\pi^4\alpha^2 I_0 N v}{\lambda^4 R^2 V}\sin^2\Phi P(q), \qquad (4.6.2)$$

where α is the polarizability, I_0 is the incident intensity, N is the number of particles, v is the scattering volume, R is the distance from scattering volume to detector, and Φ is the angle between the polarization of the incident light and the propagation direction of the scattered beam. The $P(q)$ term accounts for structural interference and is given by: $P(q) = F(q)S(q)$, where $F(q)$ accounts for destructive interference due to particle size and shape, and $S(q)$ for that due to interparticle interactions.

In most practical scenarios there are contributions to the scattered intensity from sources other than the intended sample. These include stray light, most evident at small angles, and scattering from the solvents. The scattered intensity can be broken down into three components as shown below:

$$I(\theta) = I_{\,sample}\,(\theta) + I_{\,solvent}\,(\theta) + I_{\,stray}\,(\theta) \qquad (4.6.3)$$

By measuring standards, one can subtract the extra contributions to the intensity. The sample bath is filled with toluene, which is a small molecule that scatters isotropically and thus does not significantly affect the angular distribution of the sample. We can subtract the scattering from the solvent by doing a run of pure solvent and then subtracting this intensity from that of the combined system. This gives us the scattering intensity due to the sample with small contributions from stray light, which are most significant at high q.

Previous results using small angle light scattering in Carbopol ETD 2050 found evidence of two length scales: a smaller one of approximately 0.4 μm and a larger one upwards of 6 μm, which increased with pH and concentration. The larger length scale

rapidly grew with base titration and was not able to be seen above around pH 4, as the configuration of the instrument only allowed for accurate detection of up to around 25 μm [28]. The smaller length scale was found to stay roughly constant. Fractal dimension was also found to decrease with swelling. Two length scales have also been observed in small angle neutron scattering from poly(NIPAM), a crosslinked microgel prepared with emulsion polymerization [81]. In poly(NIPAM), one length scale shrinks with temperature while the other is constant: this is thought to be associated with the existence of a dense core and a looser outer shell, which expands at low temperature [82].

In this work, we focus our light scattering on samples of Carbopol Ultrez 10. All light scattering was performed using an ALV-5000/e DLS/SLS correlator. A temperature bath was employed to keep the samples at a constant 25°C. Samples were centrifuged in glass test tubes in order to get rid of any bubbles or dust which could interfere with the scattering. Test tubes were carefully cleaned with acetone and lens paper to get rid of any exterior dust. Samples were then placed in a toluene bath. Scattering was measured across a range of angles was used from 15° to 150°. The scattering intensity distribution for one of the samples is shown in Figure 4.6.2. Note the constant rolloff, which was also seen in Carbopol ETD 2050 [81]. This shape is similar to what has been seen in aggregated silica particles and is what is expected for a distribution of clusters with an upper cutoff [83]. A fractal dimension fit of the form shown below was applied to the data [83]:

$$P(q) = \frac{P_0 \sin(D_f - 1) \arctan(q\xi)}{(1 + q^2\xi^2)^{D_f - 1/2}(D_f - 1)q\xi}. \tag{4.6.4}$$

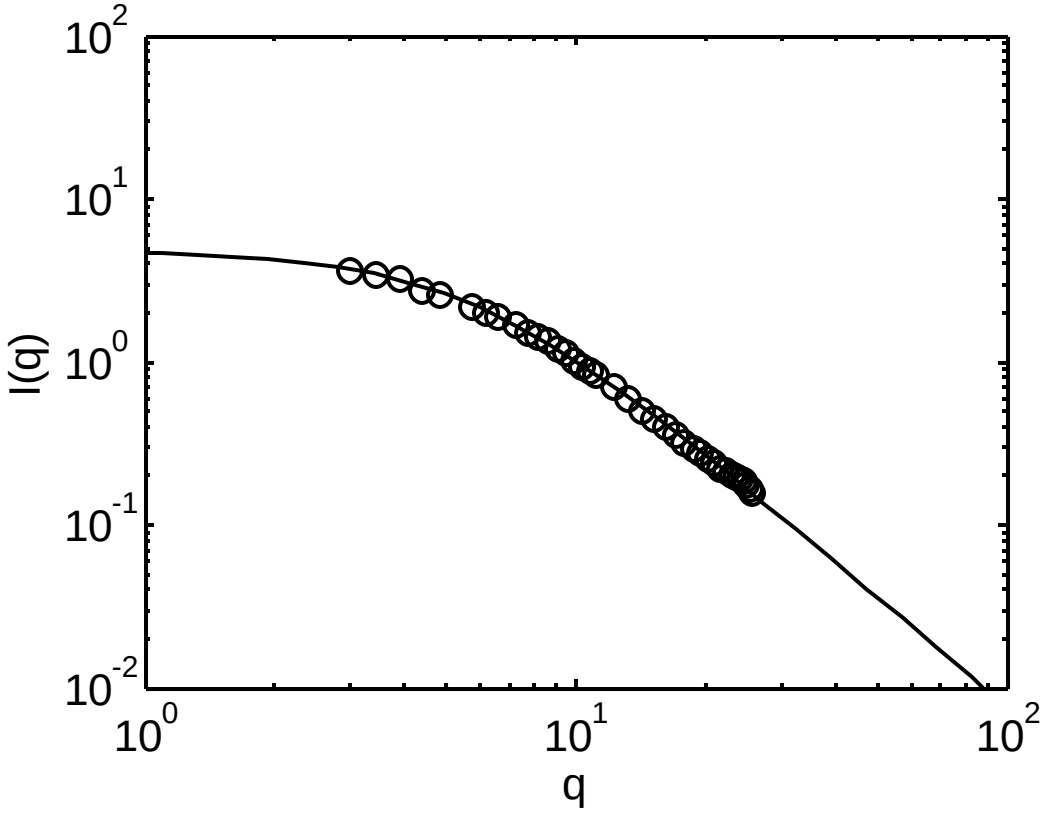

Figure 4.6.2: Plot of the intensity distribution of 0.5 wt% sample of Carbopol Ultrez 10 at ph 7. Fit parameters shown are: P_0=4.8, D_f=2.2, and ξ=0.16.

This equation is obtained by taking the Fourier transform of the correlation function $G(r)$, which we assume to be of the form of a mass fractal with fractal dimension D_f combined with a correlation term, which drops off at a characteristic length scale ξ:

$$G(r) = Ar^{(D_f-3)}e^{-\frac{r}{\xi}}. \quad (4.6.5)$$

The fractal dimensions D_f of all samples of Ultrez 10 as functions of pH are shown in Figure 4.6.3. Note that fractal dimension starts out quite high at low pH, near the space filling limit of 3, and then appears to drop down to a roughly constant value of 2.2 for all concentrations, while a slight increase is seen again at high pH. These values are similar to those seen in Carbopol ETD 2050 [28]. Errors on fractal dimension are

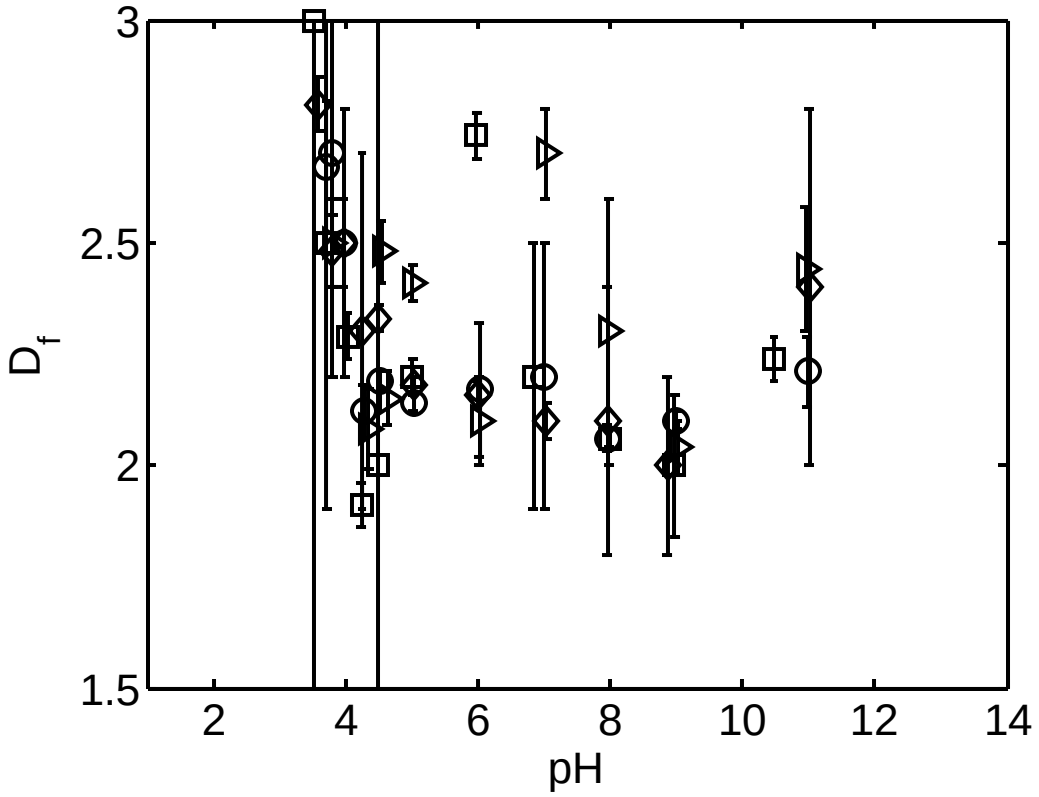

Figure 4.6.3: Plot of fractal dimension D_f for samples of Carbopol Ultrez 10 obtained from fits to the structure factor with error bars shown. Concentrations given by, 0.05%: (triangles), 0.1%: (circles), 0.2%: (diamonds), 0.5%: (squares).

quite large, this is likely correlated to errors in obtaining values for the characteristic length scale ξ which was difficult to pinpoint given the range of the data. Data from small angle light scattering of Carbopol ETD 2050 suggests that particle size and fractal dimension are inversely proportional [28]. The Carbopol Ultrez 10 data is consistent with the picture of a microgel particle which grows rapidly at low pH, stays constant at intermediate pH, and then shrinks slightly at high pH.

Fractal dimension is a good measure of structural intricacy, and as such it is useful for examining the structures of a variety of disordered systems [84]. It has been suggested that lower crosslinked gels have more branches and loose ends, and hence have

higher fractal dimensions [85]. A polymer chain that obeys Gaussian statistics is a mass fraction of dimension 2 and shows a power-law decay in structure factor. A collapsed or swollen polymer will deviate from this value [86]. A randomly branched ideal polymer has a fractal dimension of 2.29, a diffusion limited aggregate or a percolation cluster, 2.5. Randomly crosslinked networks investigated with small angle neutron scattering showed similar form, and possessed a fractal dimension of 5/3 [87]. At low scattering angle, the shape of the structure factor curve is highly dependent on crosslink density. Large scale heterogeneities are characteristic of randomly crosslinked networks [87]. Random crosslinking creates 'frozen blobs', or dense regions of crosslinks which cannot expand and stretch upon swelling and percolate the system [87]. Solvent preferentially occupies the lower crosslinked regions where local rearrangement of chains is more easily facilitated [87]. Swelling results in dilution of these clusters; the resulting density fluctuations are an artifact of random crosslinking procedures [87]. This leads to a greater degree of heterogeneity than would be seen in an equivalent uncrosslinked system, which can be observed with light scattering [48].

5: RHEOLOGY OF CARBOPOL

5.1 Introduction

In this chapter, we present and discuss the results of our bulk rheology studies of Carbopol. By examining the dependence of quantities such as the yield stress and elastic modulus on pH and concentration, we aim to draw conclusions about the underlying structure of the Carbopol microgel. We will begin by discussing the results of steady state measurements; we will discuss the hallmarks of yield-stress behaviour seen in the flow curves, plots of viscosity and stress as functions of shear rate. Then we will go on to examine the viscoelastic behaviour of Carbopol, by looking closely at the dependence of the viscoelastic moduli on both frequency and strain amplitude.

In the later sections of this chapter, we will examine the trends in rheological properties across a range of pH values and concentrations. The majority of the data shown in the first few sections of this chapter, unless otherwise indicated, comes from Carbopol ETD 2050. For the most part, the two different Carbopols showed rheological

behaviour that was qualitatively similar. In Section 5.5, we will look at the differences between Carbopol ETD 2050 and Carbopol Ultrez 10, which have different crosslink densities. In the final section, we will discuss the scaling behaviour of Carbopol gels with concentration.

5.2 Steady-State Rheology

During steady state measurements the plate is rotated at constant speed in order to give a constant shear rate as in Equation 4.3.1. The torque response of the sample, as measured at the cone, provides the necessary information for the calculation of stress and viscosity as seen in Equations 4.3.2 and 4.3.3. Measurements were taken at a range of shear rates for each sample. For some of the lowest concentration samples of both ETD 2050 and Ultrez 10 we were not able to obtain stress and viscosity data as the samples were too fluid and the transducer in the rheometer was not sensitive enough to measure a response. These samples are left out of the subsequent analysis presented in Sections 5.4 through 5.6. A characteristic plot of viscosity and stress as functions of shear rate is shown in Figure 5.2.1.

Note that for this sample it is clear that viscosity is not constant anywhere along the range of shear rates studied: this tells us very obviously that we are dealing with a non-Newtonian fluid. The divergence of the viscosity at low shear rates as seen in the this figure is typical of a yield-stress fluid. The viscosity of an ideal yield-stress fluid would theoretically diverge to infinity, however real fluids generally only approximate

this. Due this shear-rate dependent viscosity behaviour, we are unable to calculate a volume fraction using Equation 3.4.1, as this calculation assumes a constant viscosity.

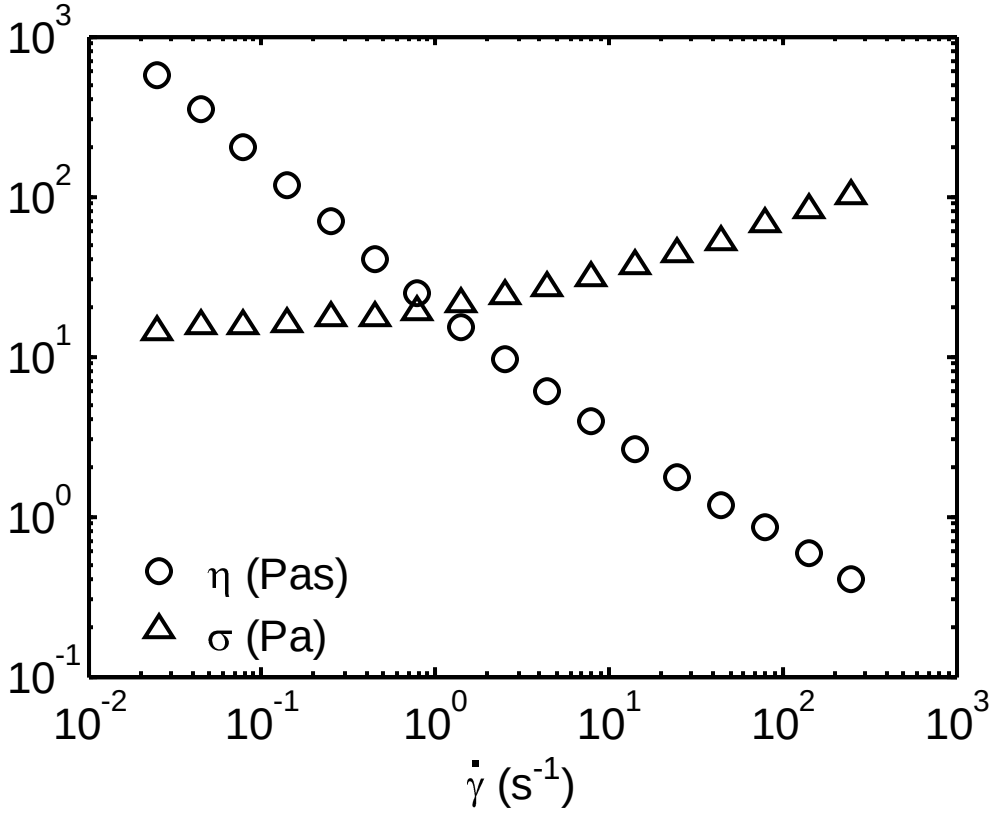

Figure 5.2.1: Plot of stress (triangles) and viscosity (circles) as a function of shear rate for a 1.5 wt%. concentration sample of Carbopol ETD 2050 at pH 3.35.

Looking at the stress curve of Figure 5.2.1, it is apparent that our sample possesses a yield stress. To further quantify the yield stress, we fit the stress data to a Herschel-Bulkley model as given in Equation 2.3.1. Slip is often a concern in the measurement of yield-stress fluids, particularly in highly viscous samples. Slip is evidenced by a dip in stress at low shear rates. Models such as the Herschel-Bulkley model do not account for slip, so its presence may distort values obtained for yield stress. In this study, we applied sandpaper to both cone and plate in an effort to minimize these

distortions and consequently did not find any significant slip artifacts in our stress curves. The fit of Herschel-Bulkley model to the stress data of Figure 5.2.1 is shown in Figure 5.2.2.

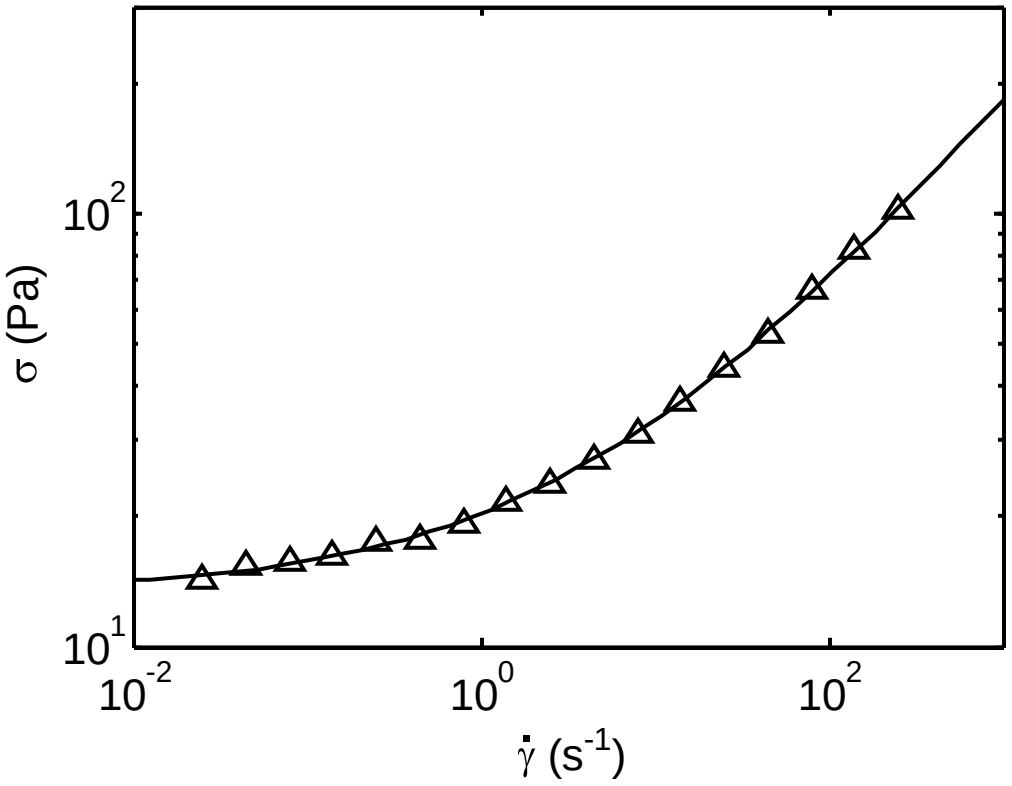

Figure 5.2.2: Plot of stress as a function of shear rate from Figure 5.2.1, with fit to the Herschel-Bulkley model shown. Fit parameters shown are: σ_0=13.4, k=6.8, and n=0.47.

These fits were performed on all measurable samples and allowed us to obtain values for the yield stresses and power law exponents over a range of conditions. The covariance matrices of the fit parameters were examined, and it was found that there was some slight correlation between the yield-stress parameter and the power-law exponent on the order of less than 0.2 for most samples. This degree of correlation is not indicative of any major problems with the model.

5.3 Oscillatory Rheology

During oscillatory tests, the plate undergoes an angular oscillation at a set amplitude and frequency. Measurements of the visco-elastic moduli can be taken by varying either amplitude or frequency. As we vary the strain amplitude, we observe a crossover between the viscous and elastic moduli. Typical results of a test performed at a constant frequency of 1 rad/s with varying strain amplitude are shown in Figure 5.3.1.

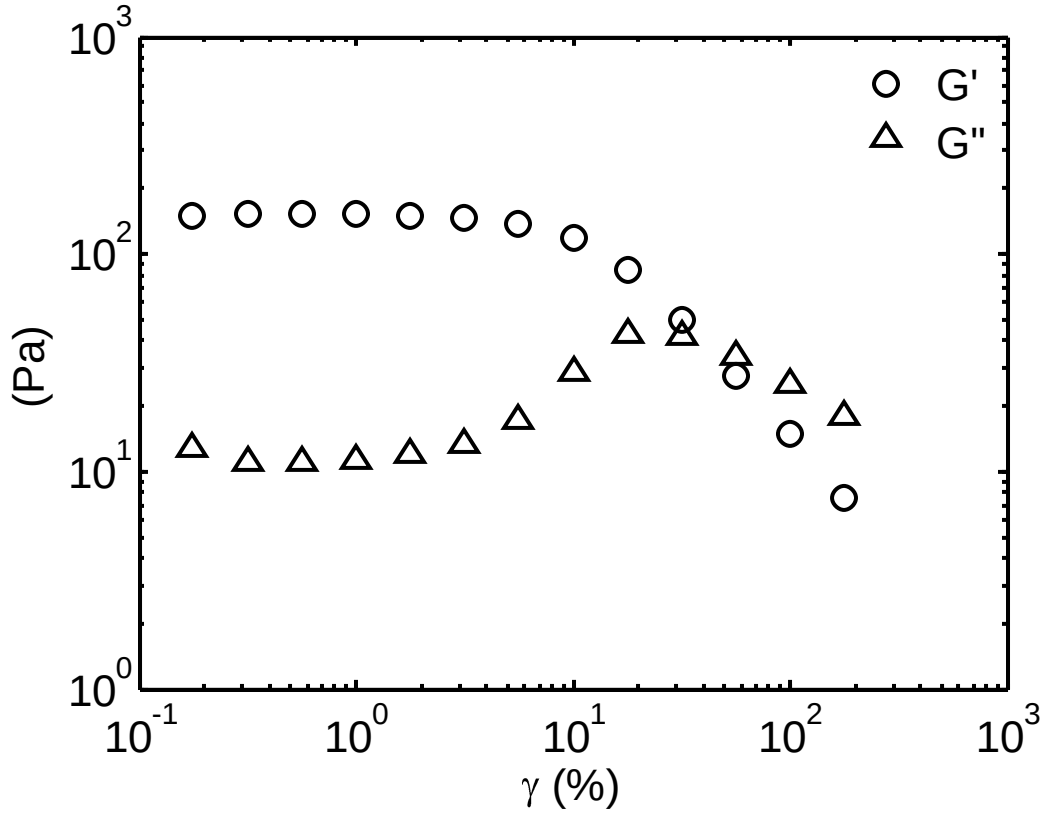

Figure 5.3.1: Plot of the viscous and elastic moduli taken over a varying strain at a constant frequency of 1 rad/s for a 1.5 wt% concentration sample of Carbopol ETD 2050 at pH 3.35.

Strain sweeps are good for establishing the range of linearity and its breakdown [34]. For small strain amplitudes, the response is typically linear [33]. Note the constant values of *G*' at low strain and the characteristic roll-off of a shear thinning fluid, which occurs at around 20% strain. Also note the maximum of *G*", which occurs just before the two moduli intersect. These moduli curves look quite comparable to those obtained from other complex fluid systems such as emulsions, and xanthan gums, as well as those of previous Carbopol studies [17,26,45,82].

For frequency sweep tests it is important that measurements are taken in the strain independent regime. In our case, we performed these sweeps at 1% strain amplitude, which as we can see from Figure 5.3.1 is in the regime where both *G*' and *G*" appear independent of strain. In Figure 5.3.2, a characteristic plot of the viscous and elastic moduli *G*' and *G*" taken as functions of driving frequency is shown.

Note that the elastic modulus is consistently larger than the viscous modulus at all frequencies measured and appears to plateau at intermediate frequencies. Meanwhile, the viscous modulus *G*" shows a characteristic minimum at around 0.2 rad/s. Similar behaviour has been observed in the rheology of hard spheres as well as in previous Carbopol studies [18,26]. In the low frequency regime, the generalized Maxwell model is applicable to Carbopol, as the moduli display a crossover where the viscous modulus peaks [88]. This crossover point of the viscoelastic moduli can be used to calculate the characteristic relaxation time of the system [55]. Unfortunately, due to the limits of the transducer sensitivity, our data does not fully cover this region. We do not observe the crossover, but we do see an increase in the viscous modulus and a decrease in the elastic

modulus at low frequencies, which hint at the existence of a crossover at lower frequencies than we

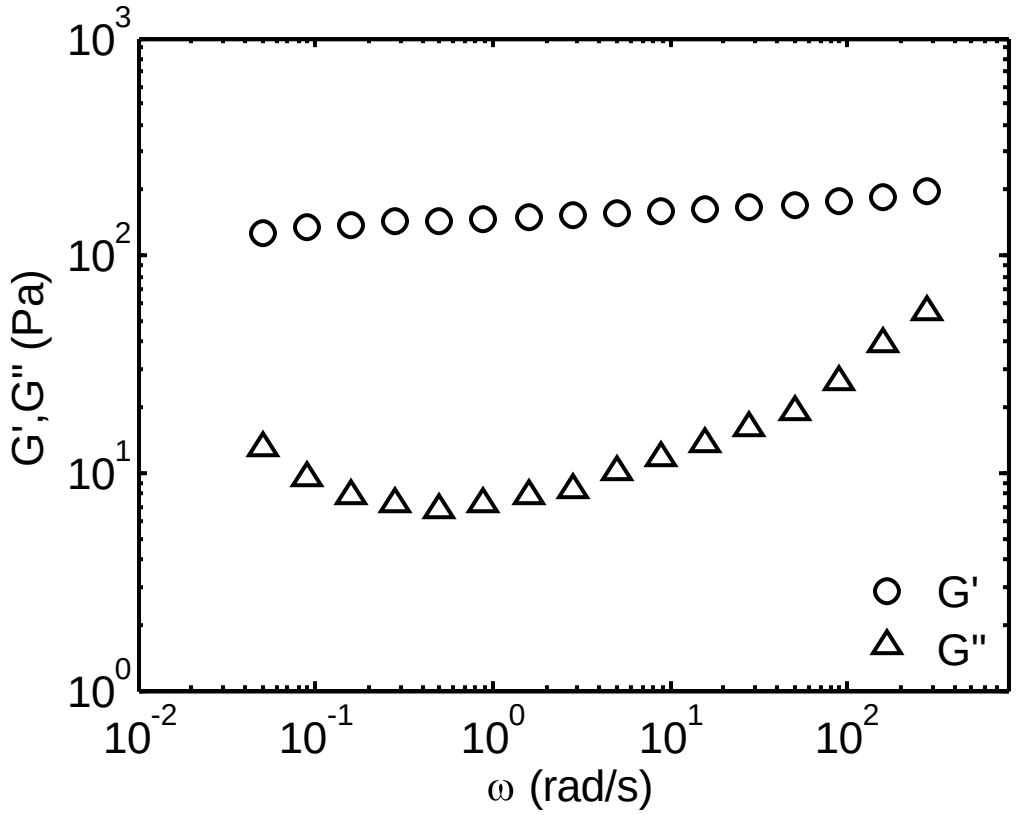

Figure 5.3.2: Plot of the elastic and viscous moduli, *G*' and *G*'' as functions of frequency taken at a constant strain amplitude of 1 wt% for a 1.5 wt % concentration sample of Carbopol ETD 2050 at pH 3.35.

are able to observe. The intermediate plateau in *G*' can be seen more dramatically in lower concentration samples as is shown in Figure 5.3.3.

The most likely explanation for this type of behaviour is as follows: at low ω the the particles will have time to deform and rearrange themselves to dissipate the applied stress. At higher ω the crosslinks and entanglements will behave as springs, as there will be not enough time for the particles to slide past each other. In this frequency regime, the

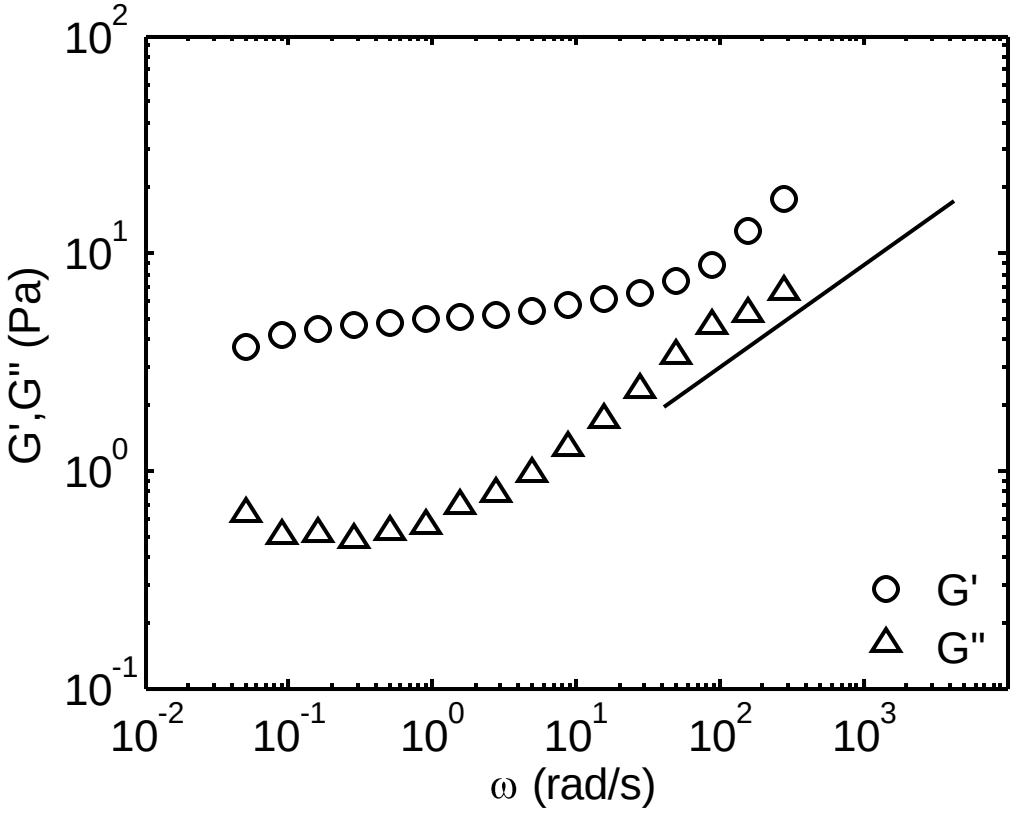

Figure 5.3.3: Plot of elastic and viscous moduli as a function of angular frequency at 1% strain amplitude for a 0.5 wt% concentration of Carbopol ETD 2050 sample at pH 3.02. Line is used to represent a power law slope of 1/2.

elastic properties will once again dominate and form a plateau. This *G'* plateau value is expected to be proportional to crosslink density [58]. At this plateau value, $G'(\omega)$ is effectively the inherent elastic modulus of the system G [40]. We see that at high frequencies the viscoelastic moduli appear to roughly increase with the square root of frequency, this is also observed in concentrated emulsions and is indicative of localized anisotropy within an overall isotropic system [40]. This type of inhomogeneity is suggested to be characteristic of the jammed state [60].

5.4 Effects of pH and Concentration

There are several important quantities that can be extracted from the curves shown in the previous sections and compared as functions of pH and concentration. A logical starting point for such comparisons is to look at the yield-stress values obtained from the fits of the Herschel-Bulkley model to the stress as a function of shear rate curve, as shown in Figure 5.2.2. The values of the calculated yield stress of each sample of Carbopol ETD 2050 are plotted as a function of pH in Figure 5.4.1.

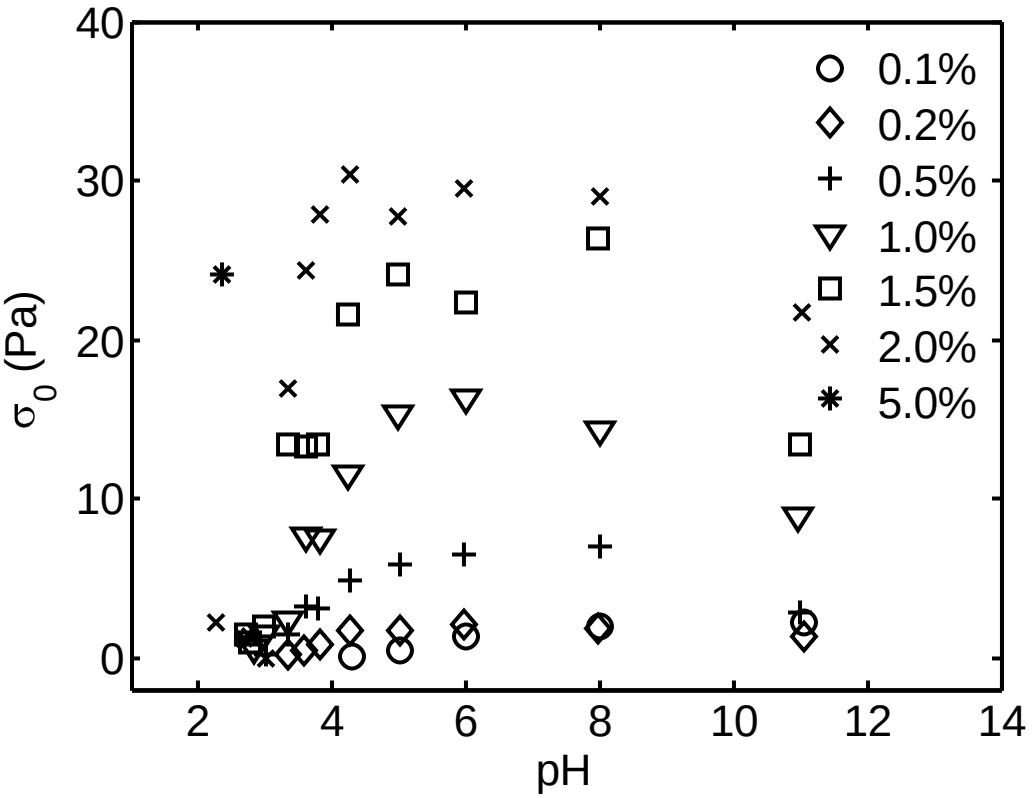

Figure 5.4.1: **Plot of yield stress σ_0 as a function of pH and concentration (see legend).**

Here we see some interesting behaviour; initially the yield stress increases with both pH and concentration, then at the highest pH values it begins to decrease slightly. This broad peak in yield stress as a function of pH is observed across all concentrations. The yield stress appears to increase monotonically with concentration; this is consistent previous Carbopol studies [27]. It is worth noting that the yield stress is quite small in some of the lower concentration samples. While a value of yield stress of 0.1 Pa is able to be measured by the rheometer, this corresponds to a fluid that will collapse under its own weight when 1 gram is spread over an area that is $1/10^{th}$ of a square meter. For most practical purposes, the yield stress of such a fluid is negligible. It should also be noted that the first two samples in the lowest concentration series did not have measurable yield stresses.

It is also worth looking at values of the Herschel-Bulkley exponent n from Equation 2.3.1. A plot of n as functions of pH for samples of Carbopol ETD 2050 is shown in Figure 5.4.2. Note that n appears to be, for the most part, independent of concentration. For an ideal Bingham fluid this exponent would be one. The values of n appear to stabilize at in the range of 0.4 to 0.6 after initial variations at low pH. Some difference in behaviour between concentrations is seen here: For lower concentrations n begins at a higher value above 0.5 and then decays and stabilizes at around 0.5, whereas in higher concentrations n appears to display a small local minimum below 0.5 and then proceeds to stabilize around a similar value. This value of 0.5 is in agreement with results obtained from previous studies of acrylate microgels [21].

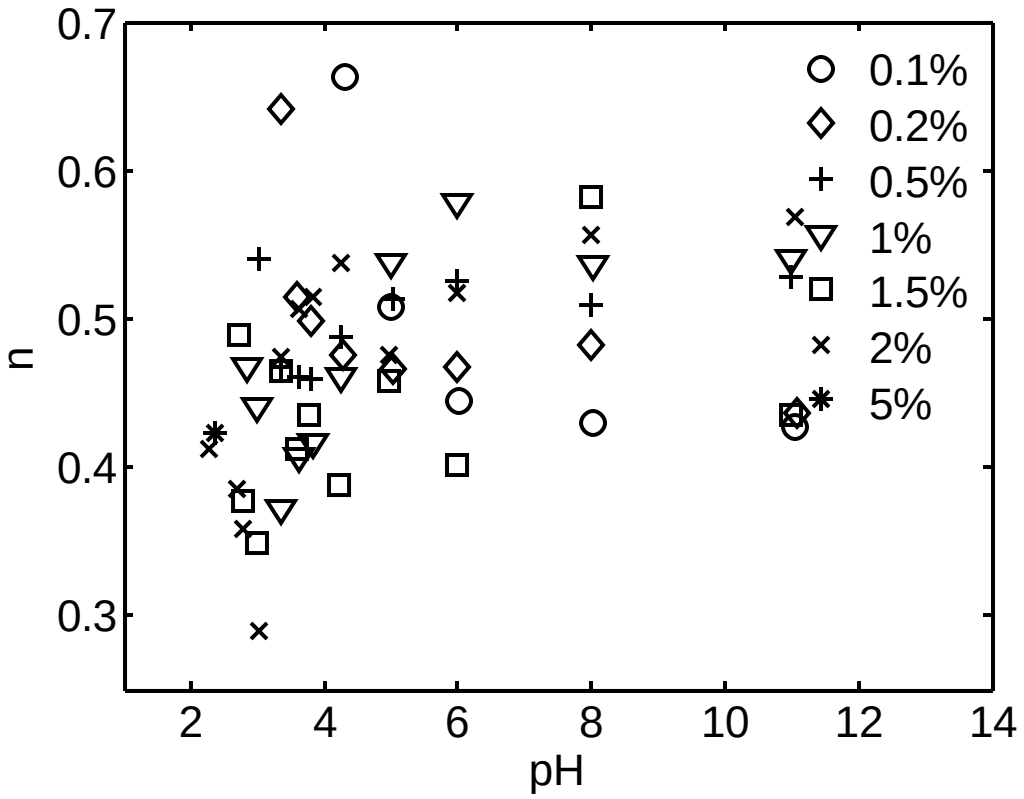

Figure 5.4.2: Plot of Herschel-Bulkley exponent *n* as a function of pH. Concentrations represented by same symbols as previous Figure.

It is also worth it at this point to compare this with the behaviour of *n* seen in samples of Carbopol Ultrez 10 as shown in Figure 5.4.3. Here we can see the low concentration behaviour described above more clearly. At low pH the exponent values are high and then they proceed to decay back down to values around 0.4-0.6.

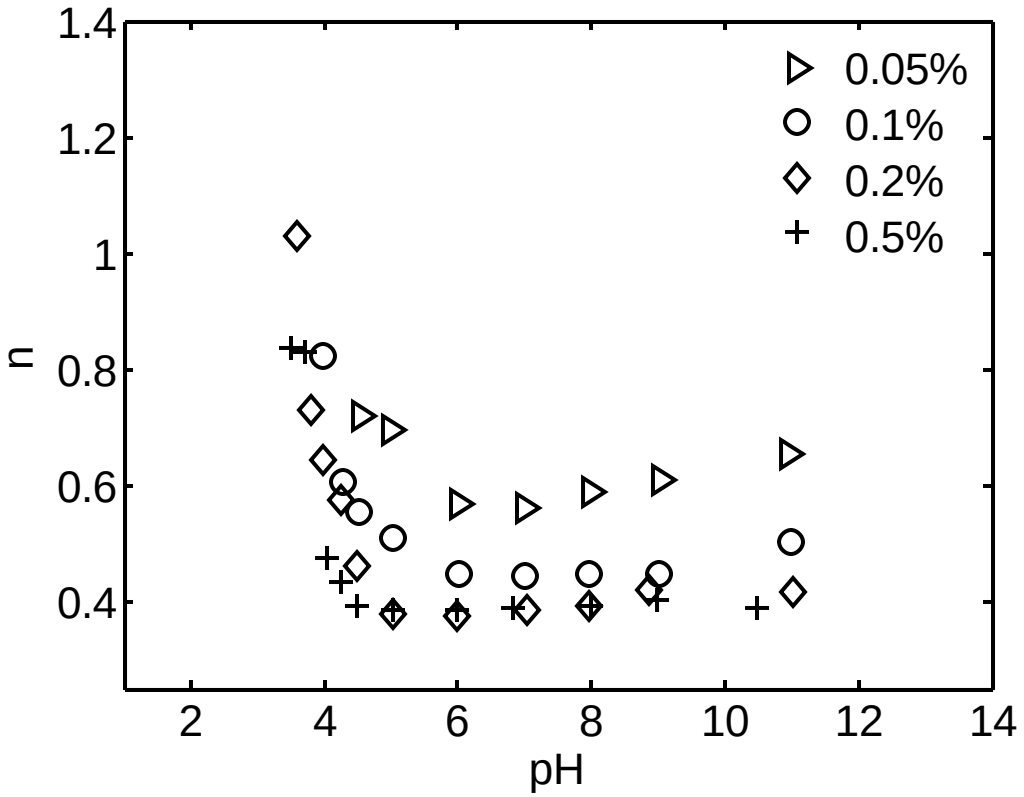

Figure 5.4.3: Plot of *n* as a function of pH for samples of Carbopol Ultrez 10.

Another quantity of interest that we can relate back to the yield stress is the critical strain γ_c. Critical strain can be thought of as the maximum deformation reachable in the solid regime. Soft materials such as Carbopol can tolerate much higher strains than hard materials, such as most metals, which break down at strains as low as 1%. [89]. Critical strain is related to the onset of flow and is also known as yield strain [37]. Critical strain is calculated from the strain sweep curves by recording the percent-strain value where the elastic modulus begins to roll off. This was defined by the point on the strain sweep curves where *G*' decays to 80% of its zero-frequency value. This was calculated by fitting manually selected points from the plateau region of the curve at low

shear rates in order to obtain a constant value of the maximum elasticity and then fitting addition manually selected points at high shear rates to a linear function and finally calculating the value of the linear function at which it reached 80% of the maximum elasticity. A plot of critical strain values for samples of Carbopol ETD 2050 is shown in Figure 5.4.4.

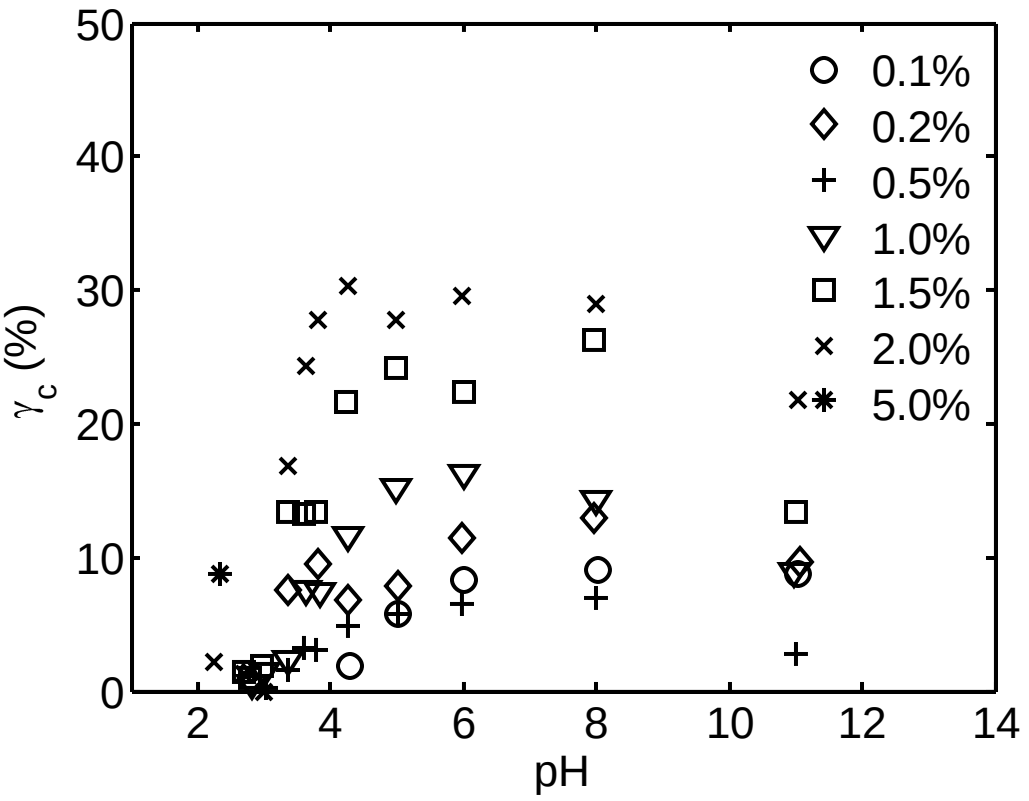

Figure 5.4.4: Plot of critical strain as a function of pH and concentration (see legend).

We see that the behaviour of the critical strain across pH and concentration is very similar to that of the yield stress. Both show strong pH dependence. Both quantities seem especially sensitive to pH at the acidic end of the spectrum; they increase very rapidly with the addition of NaOH. This is no surprise, as these two quantities should be

proportional to each other with $\sigma_0 = G\gamma_c$ [90]. It has been suggested that this formula is a better estimate of a material's yield stress than fits to a flow curve [29,73]. In Table 5.4.1, the values of yield stress for samples of various concentrations of Carbopol ETD 2050 near pH 6 are compared with values calculated from critical strain times elastic modulus. Plateau of the elastic modulus was used as an approximation of *G*.

Table 5.4.1: Values of yield stress obtained from Herschel Bulkley fits as shown in figure 5.2.2, compared to values obtained from critical strain calculation for samples of Carbopol ETD 2050 at approximately pH 6.

Concentration	σ_0 (Pa)	$G\gamma_c$ (Pa)
0.1%	1.3	1.1
0.2%	2.1	1.9
0.5%	6.5	8.2
1%	16	18
1.5%	22	24
2%	30	54

As we see from the table above the values show a rough agreement, which provides further validity to this argument.

The next quantity of interest was the plateau value of *G*' taken from the value of *G*' from the frequency sweep curves shown in figure 5.3.2 at a frequency of 1 rad/s, which is found to be in the plateau region for all samples. The *G*' values for all samples of Carbopol ETD 2050 are shown below in Figure 5.4.5.

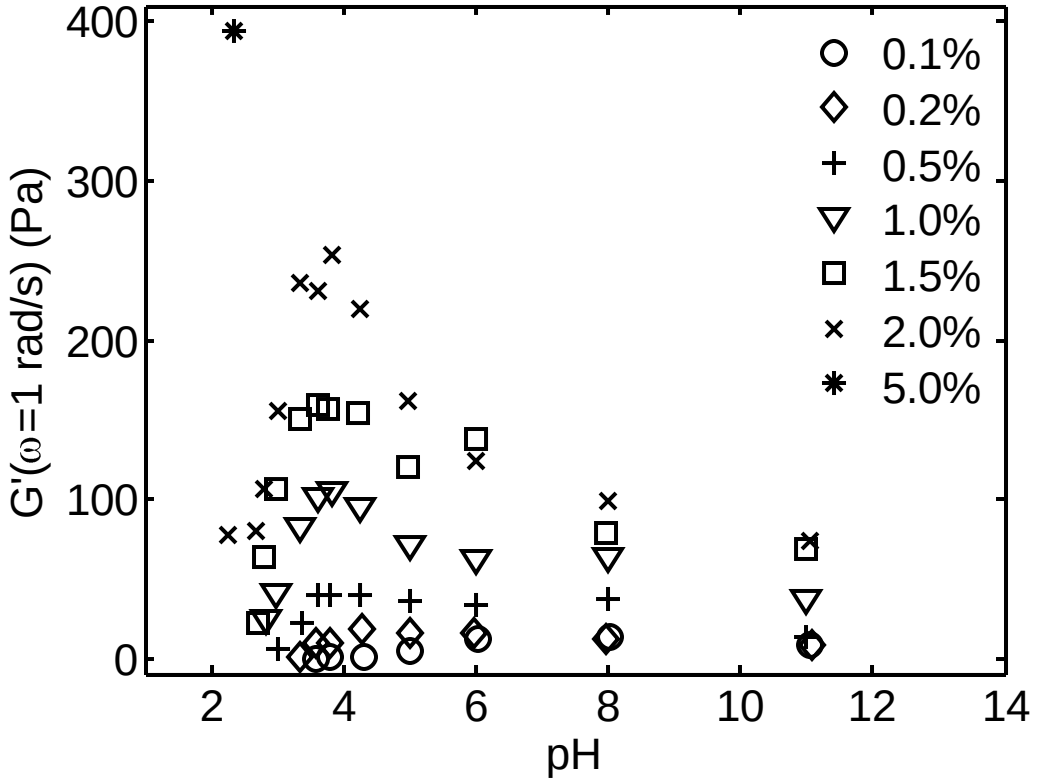

Figure 5.4.5: **Plot of the values of the elastic modulus *G*' taken at a frequency of 1 rad/s as functions of pH and concentration (see legend). Lines added to guide the eye.**

Note the appearance of a peak in *G*' for all concentrations. Interestingly the peak in *G*' is narrower and occurs at lower a pH than the peaks observed in the yield stress as seen in Figure 5.4.1. This plateau value of *G*' is a good measure of the overall elasticity of the system [44].

Another quantity that we can extract from the frequency sweep curves is the minimum value of *G*". This value was obtained from parabolic fits of manually selected points near the minima of *G*". A plot of the values as functions of pH is shown in Figure 5.4.6. Note that for certain samples, mainly the low pH samples of the lowest concentrations, the response was below the limits of transducer sensitivity therefore these

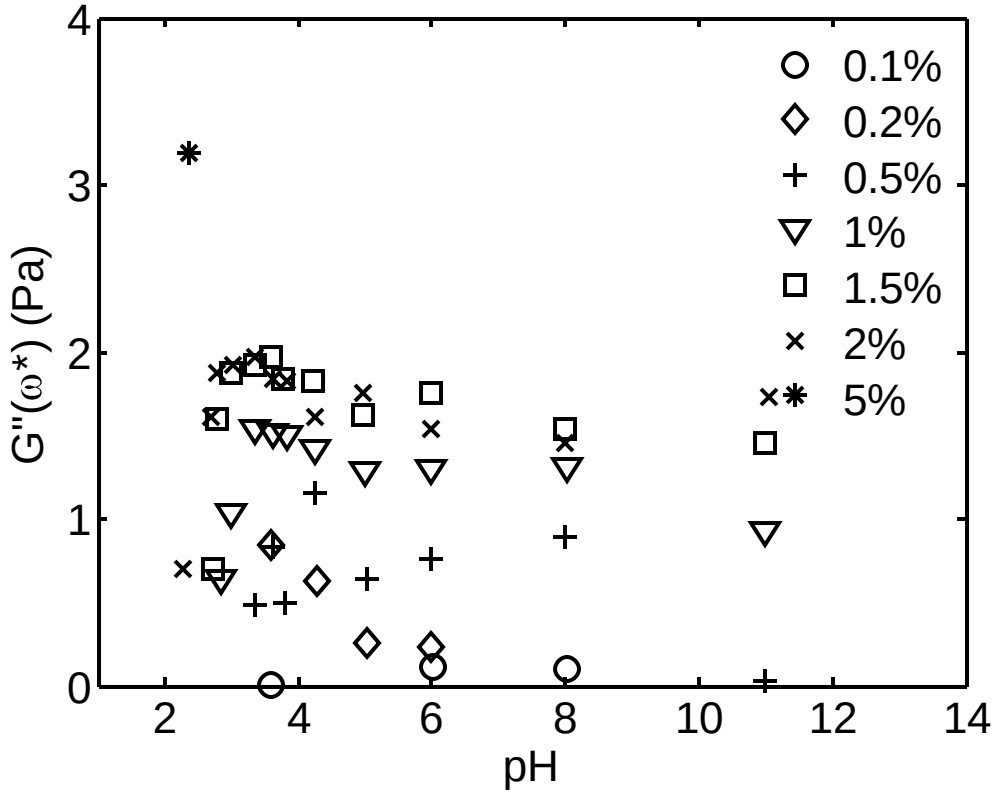

Figure 5.4.6: Plot of the minimum of G''(ω), as obtained from a parabolic fit to selected points of the frequency sweep data.

data points are excluded. Note that the minimum values of *G*" are around two orders of magnitude lower than the plateau values of the elastic modulus, which is indicative of a highly elastic material. The values increase at low pH and then remain roughly constant over intermediate and high pH. We also see that *G*" increases roughly monotonically with concentration, as is observed in emulsions [42].

Another quantity of interest was calculated from the parabolic fits of *G*"(*ω*), a frequency we shall call *ω**, which corresponds to the frequency where *G*" is at a minimum. A plot of *ω** is shown in Figure 5.4.7.

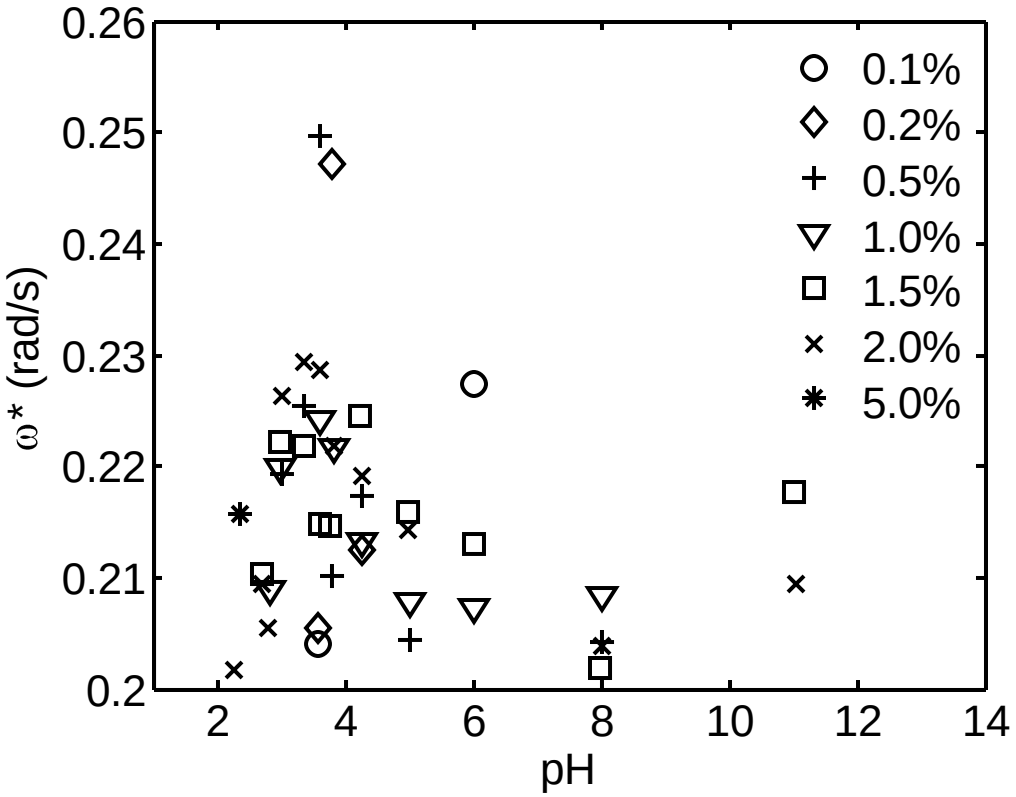

Figure 5.4.7: Plot of the frequency corresponding to the minimum of *G*''(*ω*) *ω as obtained from a parabolic fit to selected points of the frequency sweep data.**

Curiously, ω^* seems fairly independent of concentration and has a narrow peak at low pH similair to that of the elastic modulus diagram in Figure 5.4.5.

Points of interest also occurred in the strain sweep curves (see Figure 5.3.1), the most obvious was the crossover value of the viscous and elastic moduli. This was calculated from the intersection of linear fits to selected points of *G*' and *G*" near the crossover value. This value, G_C is shown in Figure 5.4.8.

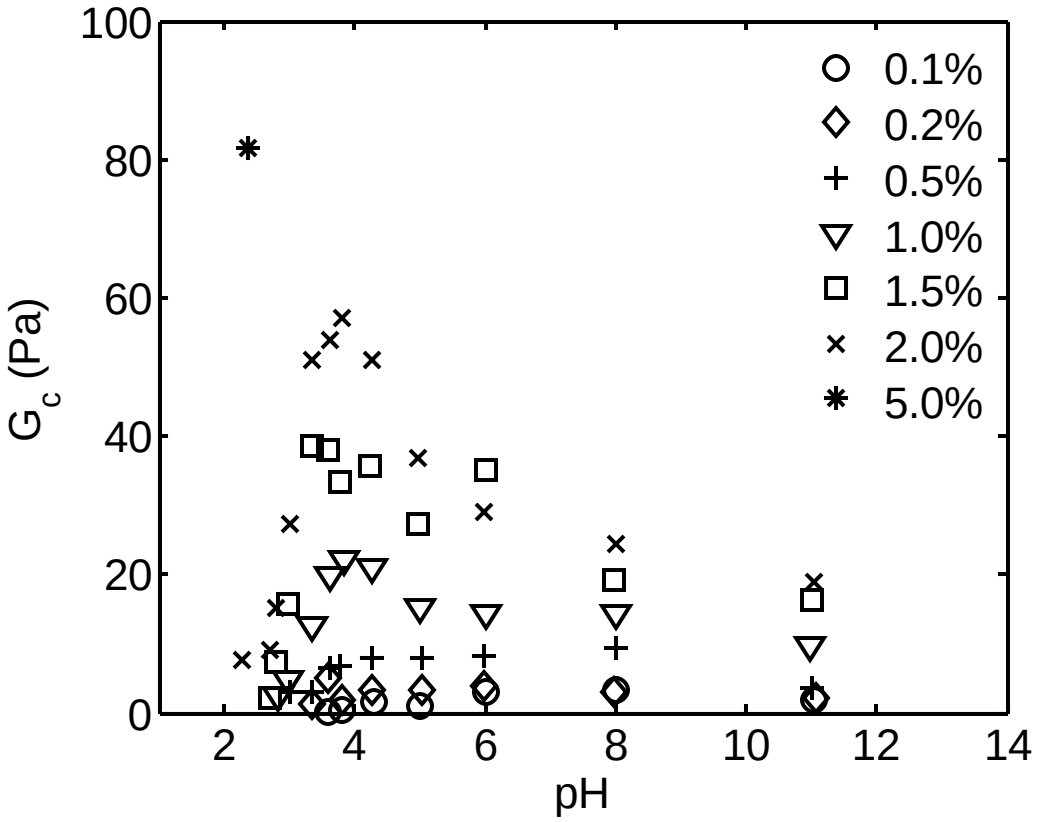

Figure 5.4.8: Plot of the value of the elastic modulus *G'* when it becomes equal to the viscous modulus *G"*.

The crossover values as functions of pH display a behaviour very similar to that of the elastic modulus plateau, with a clear peak across all samples at low pH.

5.5 Effects of Crosslink Density

In this section, we will compare the quantities of interest of Carbopol ETD 2050 seen in the previous section with those of the more highly crosslinked Carbopol Ultrez

10. Below in Figure 5.5.1 is a plot that compares the yield stress as a function of pH for three different concentrations of both ETD 2050 and Ultrez 10.

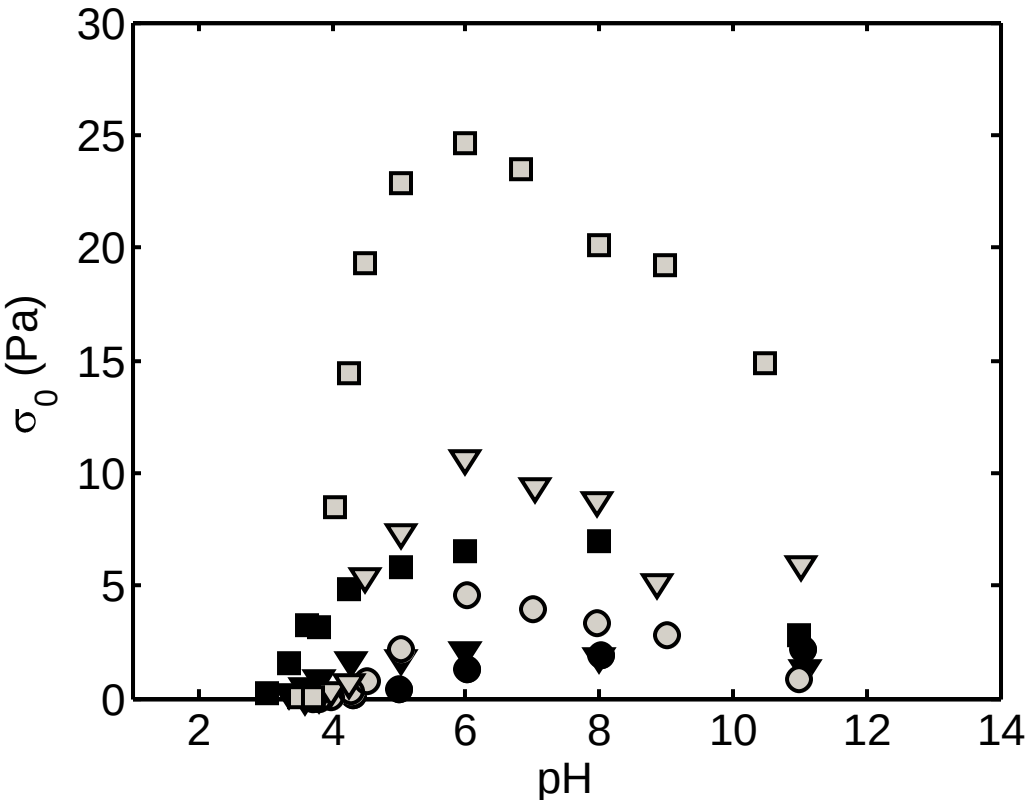

Figure 5.5.1: The yield stress as functions of pH are compared for two different Carbopols ETD 2050 (black symbols) and Ultrez 10 (gray symbols). Concentrations are represented as follows: 0.1% (circles), 0.2% (triangles), and 0.5% (squares).

Note that although the trends for the two varieties take a similar form with a soft peak at intermediate pH, the magnitude of the yield stresses for samples of the same concentration is nearly 5 times greater for Ultrez 10. This makes it clear that crosslinking has a strong effect on the yield stress. Note that at low pH, however, values of yield stress for ETD2050 are actually higher than those for Ultrez 10.

Even more dramatic are the effects of crosslinking seen in the plateau values of the elastic modulus, as seen in Figure 5.5.2.

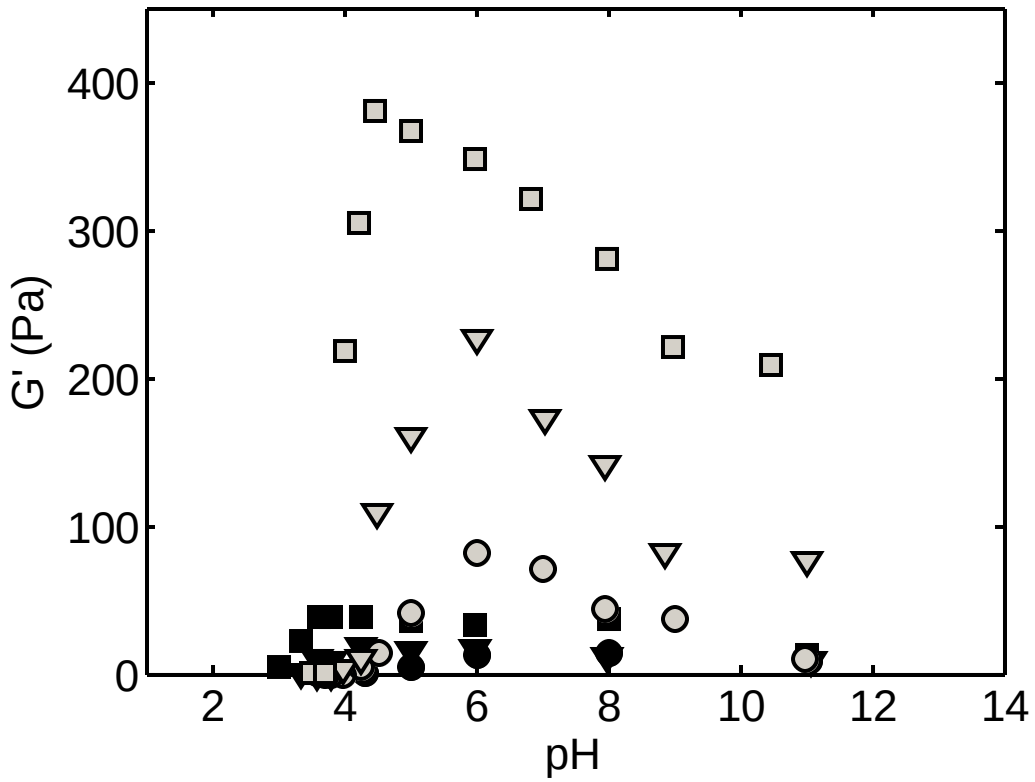

Figure 5.5.2: The elastic modulus at 1 rad/s as functions of pH are compared for two different Carbopols ETD 2050 (black symbols) and Ultrez 10 (gray symbols). Concentrations are represented as follows: 0.1% (circles), 0.2% (triangles), 0.5% (squares).

Here we see that values for Ultrez 10 are almost an order of magnitude larger than those of ETD 2050. This should come as no surprise as it was shown in Equation 3.3.2 that the elastic modulus is proportional to crosslink density. In addition, it appears that the peaks seen in the two different varieties are not centred at the same pH. Again, we see that at low pH, values for ETD2050 are higher than those for Ultrez 10.

It is also worth noting that the results for Carbopol Ultrez 10 appear to be 'smoother', or exhibit less fluctuation compared to the results for Carbopol ETD 2050. This is likely do to errors in measurement in pH, which are much larger than errors in fitting parameters. This error occurs as the pH takes a very long time, on the order of

several days, to equilibrate and readings taken too early may give a different value than the actual value at the time rheological tests were performed. For samples of Ultrez 10, an additional recheck of pH was implemented a week after the samples were prepared. We believe this extra step gives a much greater accuracy in pH, and hence accounts for the decrease in fluctuation in the data.

In order to estimate the crosslink densities of the samples we used equations 3.3.1 and 3.3.2 to calculate the crosslink densities n and mass between crosslinks M_x for the samples shown in Figure 5.5.2 at pH 6. The number of units between crosslinks l was obtained by dividing the mass between crosslinks by the molar mass of acrylic acid, which is 72.06 g/mol. The results are shown in Table 5.5.1.

Table 5.5.1: Values of crosslink density n and mass between crosslinks M_x, and units between crosslinks l calculated for samples at pH 6.

Concentration	n ($\times 10^{21}$ m^{-3})	M_x ($\times 10^6$ g/mol)	l ($\times 10^4$)
0.1% ETD 2050	3.1	200	270
0.2% ETD 2050	4.0	150	210
0.5% ETD 2050	8.2	74	100
0.1% Ultrez 10	20	30	42
0.2% Ultrez 10	55	11	15
0.5% Ultrez 10	85	7.1	9.9

Note that the crosslink densities for Ultrez 10 are roughly an order of magnitude larger than those of ETD 2050. The molar mass between crosslinks found is in agreement with earlier values found by Taylor and Bagley [23], however, they are significantly higher

than the results found by Carnali and Naser with dilute solution viscometry, which yielded values of 1450 units between crosslinks for Carbopol 940, and 3300 units for Carbopol 941 [65]. The latter results are found to be in better agreement with stoichiometry calculations [8]. Thus these values are useful for comparison between samples, but are most likely not very accurate.

5.6 Scaling Behaviour

It is useful to look for trends in the scaling of results with concentration. In our case, we attempted to see whether results scaled with concentration by looking at the yield stress divided by concentration as a function of pH for both Carbopol ETD 2050 and Ultrez10. The plot of σ_0/c for Carbopol ETD 2050 is shown in Figure 5.6.1.

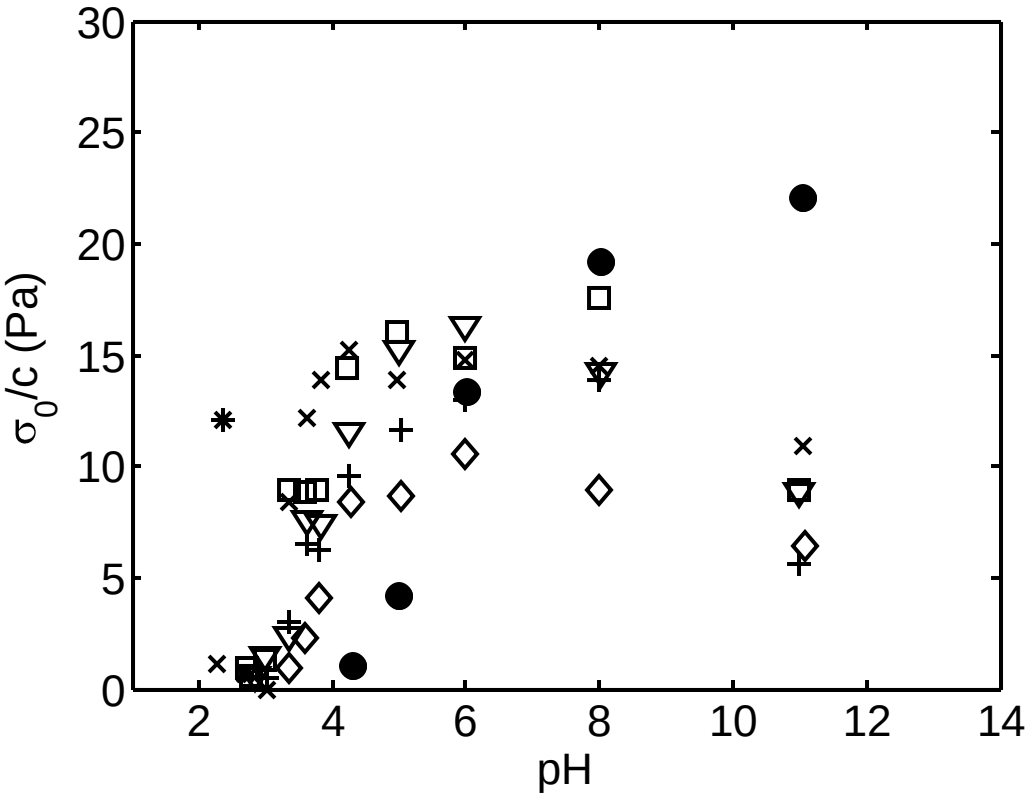

Figure 5.6.1: Plot of yield stress divided by concentration as a function of pH for samples of Carbopol ETD 2050. Concentrations designated by the following symbols: 0.1% (circles), 0.2% (diamonds), 0.5% (crosses), 1% (triangles), 1.5% (squares), 2% (xs), and 5% (asterisks). Lowest concentration shown with filled symbols for emphasis.

In the above figure, we see that the curves very roughly collapse, except for the lowest concentration, which is higher in magnitude and peaks at a later pH. Similar behaviour is seen in samples of Carbopol Ultrez 10, as shown in Figure 5.6.2.

The fluctuations in these scaling curves may be associated with an error induced in the determination of pH. Further analysis of the data by implementing regularized curve fitting to adjust the pH values and smooth out these fluctuations may give improved scaling.

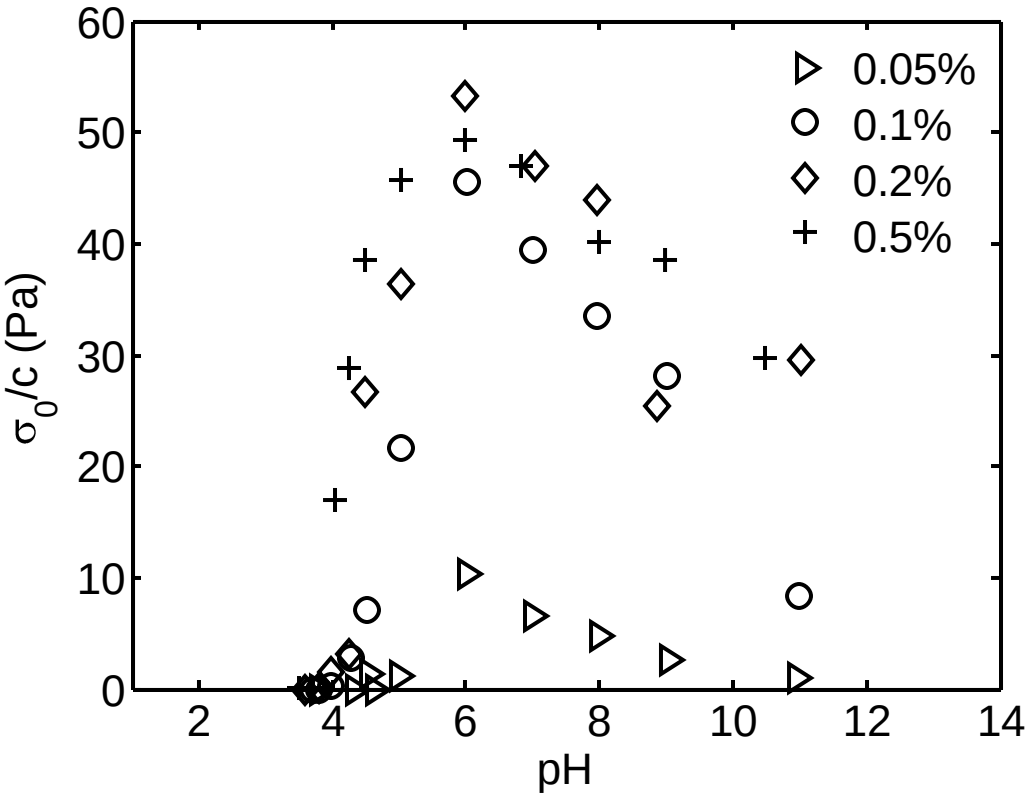

Figure 5.6.2: Plot of yield stress divided by concentration as a function of pH for samples of Carbopol Ultrez 10.

Here again we see that that the curves roughly collapse except that of the lowest concentration sample, which in this case is smaller than the rest. This is indicative of a structural change, which occurs at a concentration near 0.05-0.1 wt%.

After considering this scaling in the yield stress, we then look for evidence of scaling in the plateau modulus *G*'. In Figure 5.6.3 we show a plot of *G*'/*c* as a function of pH for samples of Carbopol ETD 2050.

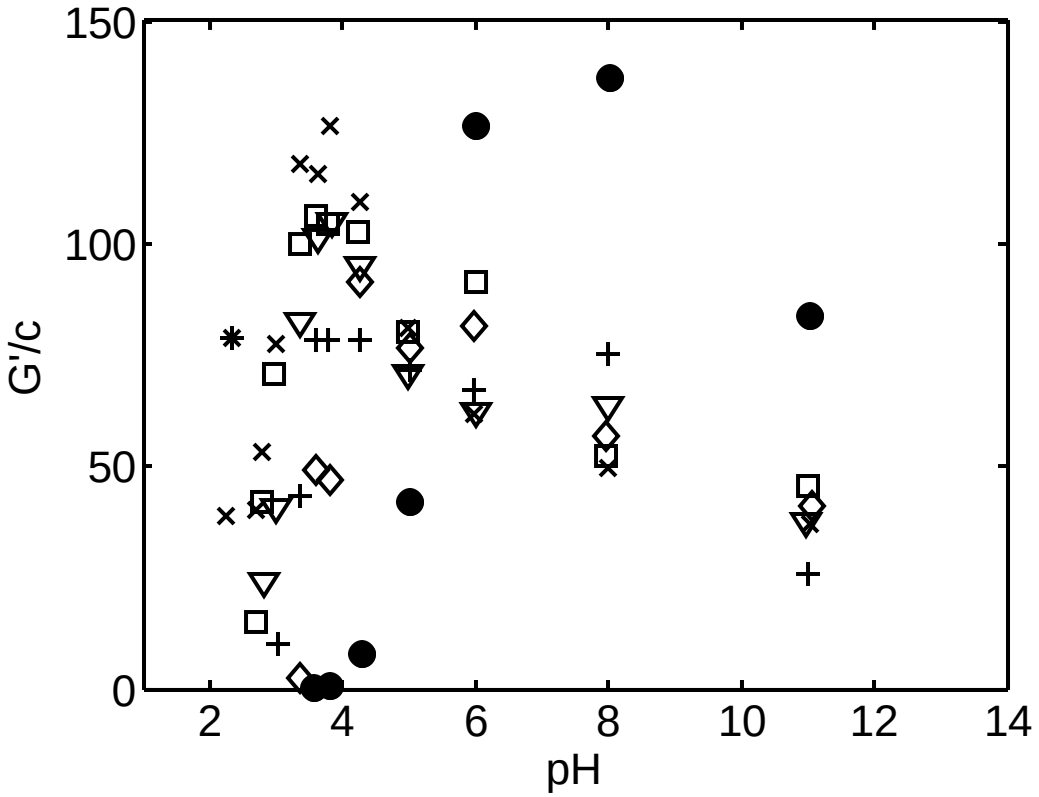

Figure 5.6.3: Plot of plateau modulus divided by concentration as a function of pH for samples of Carbopol ETD 2050. Concentrations designated by the following symbols: 0.1% (circles), 0.2% (diamonds), 0.5% (crosses), 1% (triangles), 1.5% (squares), 2% (xs), and 5% (asterisks). Lowest concentration shown with filled symbols for emphasis. Lowest concentration shown with filled symbols for emphasis.

In the above figure we see that the curves roughly collapse, with the exception of the lowest concentration samples, most markedly, the lowest concentration of 0.1%, which peaks at a much higher pH. Carbopol Ultrez 10 displays similar behaviour as seen in Figure 5.6.4.

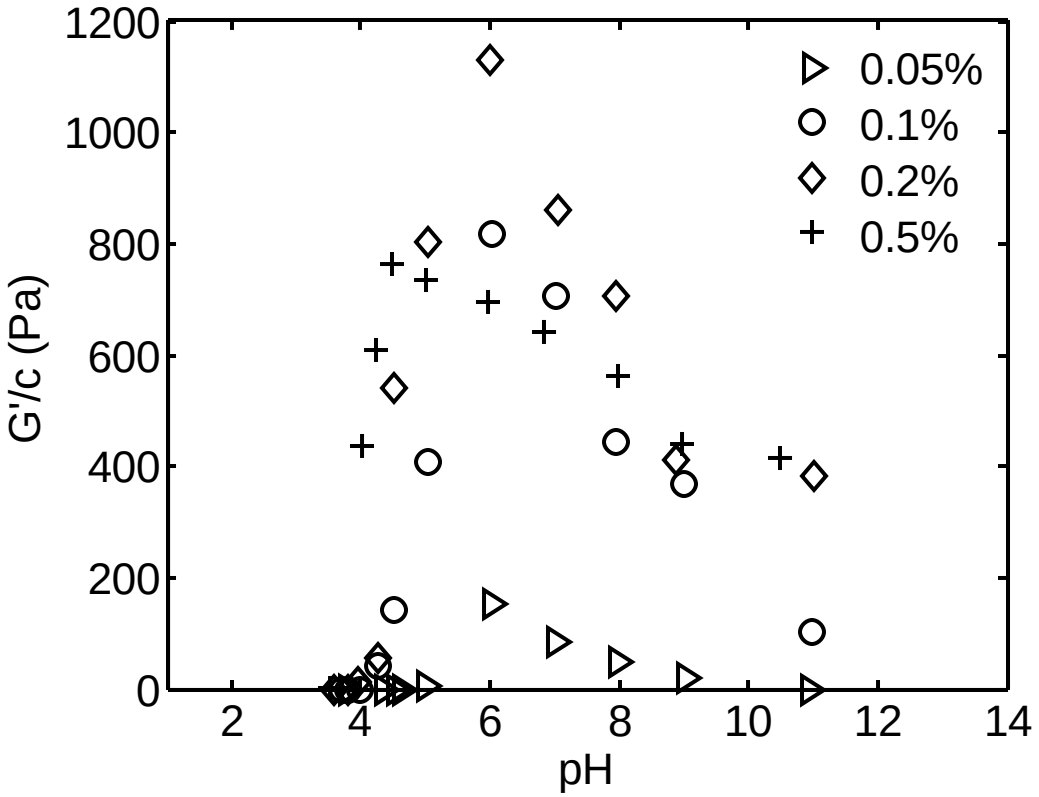

Figure 5.6.4: Plot of plateau modulus divided by concentration as a function of pH for samples of Carbopol Ultrez 10.

Here we find the lowest concentration sample differs from the rest by having *G*'/*c* significantly smaller in magnitude. We also see that the highest concentration sample peaks at a lower pH. This is again suggestive of a transition occurring in the structure within the range of the concentrations we have studied. We will expand upon this further in the next chapter.

6: DISCUSSION

In this study, we have observed competing effects of pH and concentration on the viscoelastic properties of Carbopol. This was evidenced by the broad peaks seen in both the yield stress and elastic modulus as functions of pH. These changes in rheology are likely related to changes in the underlying microstructure of the gel. We know from previous studies with small angle light scattering that as ions are added the polymers swell significantly, by up to three orders of magnitude in volume. These swollen particles occupy a greater volume fraction, which increases the effects of jamming and makes the sample more like an elastic solid. The particles become larger and larger with base titration until they no longer have room to expand and become compressed against each other. After the ions within the particles become fully dissociated the particles begin to experience a net inward osmotic pressure, which causes them to compress. Many of the key rheological quantities we have examined seem to be intimately tied with particle size and volume fraction. The behaviour observed is consistent with a model of changing particle sizes and volume fractions with pH and concentration.

At low pH, the unmodified polymers are tightly bound and not space-filling, however, evidence of a yield stress and a plateau in the elastic modulus even at these low concentrations indicates that the suspension has some sort of mesostructure which spans the sample. The most likely structure is that of a percolated network, akin to what would be seen in dilute hard spheres. Our bulk rheology and previous microrheology supports this picture. In a study by Oopong *et al.* two distinct regions of mobility of tracer particles are seen in samples at these concentrations, which indicate that there are ponds of solvent within a percolated gel network [71].

As ions are added, they preferentially enter the negatively-charged particles, this leads to an imbalance in osmotic pressure and water is drawn into the particles and they swell. Light scattering has shown that the particles increase in volume very quickly with base titration. At a certain point the swelling leads the particles to occupy a volume fraction higher than the limit of random close packing . At this point, in order to swell further, the particles must begin to compress against each other. Near the onset of this space filling and compression, we see some changes in behaviour: for lower concentration samples, peaks in yield stress and elastic modulus do not increase as quickly with base titration at low pH likely because they are not yet swollen enough to be space filling. Some of the lowest-concentration samples were found to have no measurable yield stress in their pH-unmodified form, which indicates that they may not form any type of structure at this stage. Above a certain concentration, 0.1 wt% for ETD 2050 or 0.05 wt% for Ultrez10, we see clear yield-stress peaks at the same pH range and concentration. This is indicative of these samples all forming a similar space-filling structure at maximum swelling. In the microrheological study mentioned above it was

observed that near neutral pH as concentration was increased the tracer particles became trapped [71]. This is indicative of the compressed gel particles forming an elastic solid [71].

Our data shows highest values of yield stress and elastic modulus at intermediate pH values across all concentrations. This trend of increasing yield stress with increasing concentration at constant pH supports the idea of a jamming effect due to higher volume fraction at higher pH. The compression of the elastic particles leads to a very strongly jammed structure, as evidenced by the high yield stresses and elastic moduli seen in this regime. This is because the particles are tightly packed and do not easily move past each other and rearrange; instead they dissipate perturbations elastically by deforming.

When the volume fraction reaches its highest level, where it approaches unity, jamming is at its greatest. In this state, the system is effectively an interconnected network, and the value of the plateau of the elastic modulus is likely a good indicator of overall system crosslink density [24,91]. Near this maximum volume fraction, particles can't swell much but continue to compress against each other. In this space filling regime the structure has no room to undergo any significant changes; this is supported by the broad nature of the peaks in yield stress.

At high pH, osmotic effects may lead to a deswelling of the particles. We believe this deswelling is not nearly as radical as the initial swelling. The particles are not found to return to their initial sizes. Rather, this slight shrinking simply leads to a relaxation of the structure, or a lowering of the compression between particles, and thus allows for greater particle motion in response to perturbations.

Strong concentration effects are also seen. It is likely that the lowest concentration samples reach the space filling limit much later than high concentrated samples. These samples possibly remain as percolated networks, at neutral pH, whereas higher concentration samples quickly become strong compressed networks. This concept is illustrated below in Figure 6.1.

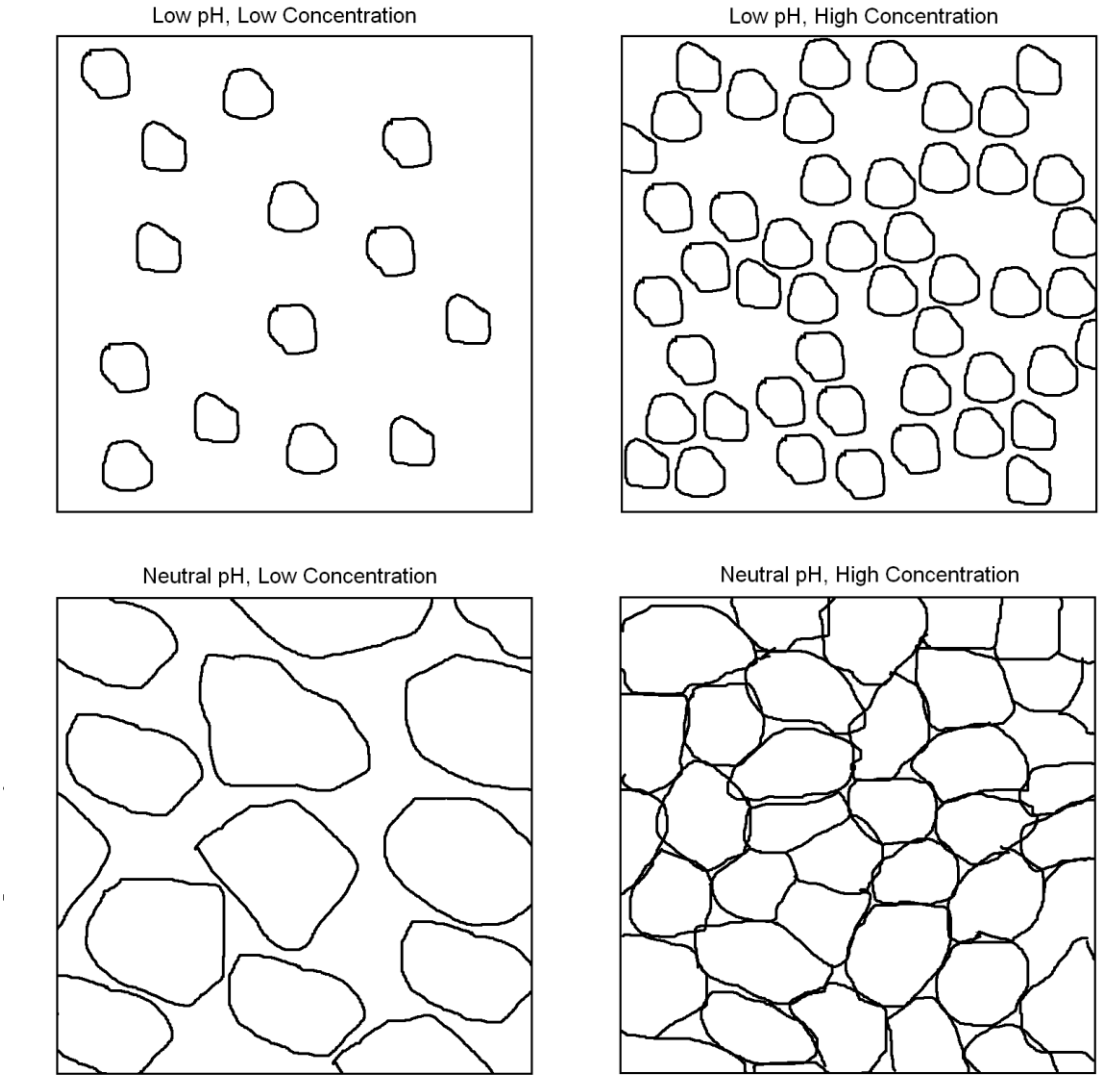

Figure 6.1: Illustration of the proposed effects of base titration on low and high concentration Carbopol gels.

This model is best supported by the concentration scaling curves of Figures 5.6.1-5.6.4, where higher concentration samples roughly collapse, yet lower concentrations indicate a different behaviour. This suggests that the lowest concentration samples of both varieties of Carbopol studied have a fundamentally different mesostructure: the elastic modulus should scale with concentration for a network, so from the scaling curves we can assume at maximum swelling the system closely represents a network for all but the lowest concentration samples.

Crosslinking also seems to affect rheological properties significantly. Flory states that there is an inverse relationship between swelling capacity and crosslink density [49]. Thus, at lower pH, the highly crosslinked gels do not swell as quickly and thus display smaller values in both yield stress and elastic modulus than similar concentrations of lower crosslinked gels at the same pH. However, at higher pH, both systems will inevitably reach a volume fraction that approaches unity and the higher rigidity of the more crosslinked particles leads to a higher yield stress and elastic modulus. This is because more rigid particles do not deform in order to flow past each other as easily, and this leads to a higher yield stress [91]. Ultrez 10 was found to have peaks in both yield stress and elastic modulus at higher pH values than ETD 2050. While at lower pH ETD 2050 showed higher values of the elastic modulus and yield stress, the maximum values overall of Ultrez 10 were much larger; the system simply did not swell as much and did not reach the space filling limit until higher pH.

Similar scaling behaviour has been seen in aqueous starch systems. In these systems, starches begin to swell and take on water at a certain temperature, below which they are rigid particles governed only by excluded volume interactions like hard spheres

[91]. Starches are elastic, that is they display a higher value of *G*' than *G*", and they also posses yield stresses. Like Carbopol, these particles are highly deformable, and space filling occurs at high concentrations [91]. It has been shown that less swellable granules have lower elasticity and viscosity than higher swelling granules at low concentration, whereas at higher concentrations the opposite is true [91]. For systems of deformable particles it appears that in the dilute regime, volume fraction is the dominant predictor of rheological behaviour, whereas in the concentrated regime, behaviour appears to be more dependent on particle rigidity [91].

7: CONCLUSION AND OUTLOOK

In this study, we have examined the rheological behaviour of Carbopol gels over a wide range of conditions. We found that pH, concentration, and crosslinking density all have strong effects on the rheology of Carbopol gels. The strongest structures, as evidenced by high values of the yield stress and elastic modulus, were found at intermediate pH and high crosslinking densities and concentrations. We argue that these strong structures consist of a space filling paste of compressed particles, while the weaker structures seen at lower pH and concentration consist of a hard sphere-like percolated network of particles. We see evidence of a transition between the two types of structures described above when rheological data is scaled with concentration. Additional weakening of the structures was observed at high pH and we propose that this is due to an osmotic deswelling mechanism.

Light scattering results suggest that the rheological properties of Carbopol are closely tied with particle swelling and effective volume fraction as controlled by pH and concentration. While we see indications of a change in behaviour from a percolated

structure to a space filling network with increased concentration in the rheological data, unfortunately, Carbopol particles swell so much as to render their size too large to be detected by conventional light scattering methods above a certain pH. Thus while we can watch the particles swell from their pH-unmodified state to beyond the limits of the light scattering apparatatus, we have not been able to observe their proposed critical swelling and deswelling beyond this point.

Further studies of interest might include various techniques aimed at determining particle sizes at intermediate and higher pH. One promising approach would be to fluorescently dye the Carbopol particles and attempt to observe the microstructure in three dimensions using fluorescent microscopy. This could be done with a small cationic fluorescent dye; the hope would be that the dye particles would be drawn into the particles and induce swelling in a way analogous to sodium and that by examining a dilute sample of Carbopol a particle size could be extracted from images taken with a fluorescence microscope. If this technique proved successful, a much more detailed picture of the structure and size of the individual sponges could be obtained. Additionally more bulk rheological tests, such as strain controlled measurements, could be implemented to further characterize the rheological behaviour of Carbopol microgels, and to compare with the results obtained in recent works on similar microgels[19, 61]. Also promising is the application of further microrheological techniques to Carbopol. Particle tracking with fluorescence microscopy, as was performed by Oopong *et al.* on Carbopol ETD 2050, has yet to be applied to samples of Carbopol Ultrez 10 [71, 74]. Additional microrheological approaches also have a potential to yield new information about Carbopol's structure, such as active microrheology with optical tweezers. This

technique could be employed to probe the structure of Carbopol by studying the forces on a small particle being dragged through a sample. By actively controlling the tracer particle we may be able to penetrate regions of the gel that were not accessible with passive techniques.

In addition it would be useful to prepare additional samples under the same conditions and redo the rheology tests, in order to ensure the reproducibility of our results. It would also be useful to examine data taken on the cone and plate rheometer without sandpaper applied in order to ensure that it is not significantly distorting our rheological data.

While we have obtained a great deal of information about Carbopol's rheological behaviour in this study, much of its underlying structure still remains a mystery, which is ripe for further examination with many of the aforementioned techniques.

REFERENCE LIST

[1] D. Sikorski, H. Tabuteau, and J. R. de Bruyn, Motion and shape of bubbles rising through a yield-stress fluid, Journal of Non-Newtonian Fluid Mechanics **159**, 10-16 (2009).

[2] M. Hariharaputhiran, R. S. Subramanian, G. A. Campbell, and R. P. Chhabra, The settling of spheres in a viscoplastic fluid, Journal of Non-Newtonian Fluid Mechanics **79**, 87- 97 (1998).

[3] D. D. Atapattu, R. P. Chhabra, and P. H. T. Uhlherr, Creeping sphere motion in Herschel-Bulkley fluids: flow field and drag, Journal of Non-Newtonian Fluid Mechanics **59**, 245-265 (1995).

[4] A. Amanullah, S. A. Hjorth, and A. W. Nienow, A new mathematical model to predict cavern diameters in highly shear thinning, power law liquids using flow impellers, Chemical Engineering Science **53**, 455-469 (1998).

[5] I. P. T. Moore, G. Cossor, and M. R. Baker, Velocity distributions in a stirred tank containing a yield stress fluid, Chemical Engineering Science **50**, 2467-2481 (1995).

[6] H. Tabuteau, P. Coussot, and J. R. de Bruyn, Drag force on a sphere in steady motion through a yield-stress fluid **51**, 125-137 (2007).

[7] M. Muramatsu, K. Kanada, A. Nishida, K. Ouchi, N. Saito, M. Yoshida, A. Shimoaka, T. Ozeki, H. Yuasa, and Y. Kanaya, Application of Carbopol to controlled release preparations I. Carbopol as a novel coating material, International Journal of Pharmaceutics **199**, 78-83 (2000).

[8] Noveon Pharmaceuticals, Noveon Polymers Technical Bulletins (2002).

[9] D. Bonn, and M. M. Denn, Yield stress fluids slowly yield to analysis, Science **324**, 1401-1402 (2009).

[10] P. Moller, A. Fall, V. Chikkadi, D. Derks, and D. Bonn, An attempt to characterize yield stress fluid behaviour, Philosophical Transactions of the Royal Society A **367**, 5139-5155 (2009).

[11] M. Cloitre, R. Borrega, and L. Lieber, Rheological aging and rejuvenation in microgel pastes, Physical Review Letters **85**, 4819-4822 (2000).

[12] G. P. Roberts, and H. A. Barnes, New measurements of the flow-curves for Carbopol dispersions without slip artefacts, Rhelogical Acta **40**, 499-503 (2001).

[13] H. A. Barnes, and K. Walters, The yield stress myth?, Rheological Acta **24**, 323-326 (1985).

[14] H. A. Barnes, The yield stress-a review or 'παντα ρει'-everything flows?, Journal of Non-Newtonian Fluid Mechanics **81**, 133-178 (1999).

[15] S. J. Curran, R. E. Hayes, A. Afacan, M. C. Williams, and P.A. Tanguy, Properties of carbopol solutions as models for yield-stress fluids, Journal of Food Science **67**, 176-180 (2002).

[16] P. C. F. Møller, A. Fall, and D. Bonn, Origin of apparent viscosity in yield stress fluids below yielding, Europhysics Letters **87**, 38004 (2009).

[17] T. G. Mason, J. Bibette, and D. A. Weitz, Yielding and flow of monodisperse emulsions, Journal of Colloid and Interface Science **179**, 439-448 (1996).

[18] T. G. Mason, and D. A. Weitz, Linear viscoelasticity of colloidal hard sphere suspensions near the glass transition, Physical Review Letters **75**, 2770-2773 (1995).

[19] H. M. Wyss, K. Miyazaki, J. Mattsson, Z. Hu, D. R. Reichman, and D. A. Weitz, Strain-rate frequency superposition: a rheological probe of structural relaxation in soft materials, Physical Review Letters **98**, 238303 (2007).

[20] P. Sollich, F. Lequeux, P. Hébraud, and M. E. Cates, Rheology of soft glassy materials, Physical Review Letters **78**, 2020-2023 (1997).

[21] M. Cloitre, R. Borrega, F. Monti, and L. Leibler, Glassy dynamics and flow properties of soft colloidal pastes, Physical Review Letters **90**, 068303 (2003).

[22] W. H. Fischer, W. H. Bauer, and S. E. Wiberley, Yield stress and flow properties of carboxypolymethylene-water systems, Transactions of the Society of Rheology **5**, 221-235 (1961).

[23] N. W. Taylor, and E. B. Bagley, Rheology of dispersions of swollen gel particles, Journal of Polymer Science **13**, 1133-1144 (1975).

[24] N. W. Taylor, and E. B. Bagley, Tailoring closely packed gel-particle systems for use as thickening agents, Journal of Applied Polymer Science **21**, 113-122 (1977).

[25] F. K. Oopong, L. Rubatat, B. J. Frisken, A. E. Bailey, and J. R. de Bruyn, Microrheology and strucute of a yield-stress polymer gel, Physical Review E **73**, 041405 (2006).

[26] J. M. Piau, Carbopol gels: elastoviscoplastic and slippery glasses made of individual swollen sponges meso- and macroscopic properties, constitutive equations and scaling laws, Journal of Non-Newtonian Fluid Mechanics **144**, 1-29 (2007).

[27] J.-Y. Kim, J.-Y. Song, E.-J. Lee, and S.-K. Park, Rheological properties and microstructures of Carbopol gel network system, Colloid and Polymer Science **218**, 614-623 (2003).

[28] D. Lee, I. A. Gutowski, A. E. Bailey, J. R. de Bruyn, and B. J. Frisken, Investigating the structure of a yield-stress polymer gel by light scattering, In Preparation.

[29] R. J. Ketz, Jr., R. K. Prud'homme, and W. W. Graessley, Rheology of concentrated microgel solutions, Rheological Acta **27**, 531-539 (1988).

[30] H. N. Naé, and W. W. Reichert, Rheological properties of lightly crosslinked carboxy copolymers in aqueous solutions, Rheological Acta **31**, 351-360 (1992).

[31] R. Borrega, M. Cloitre, I. Betremieux, B. Ernst., and L. Leibler, Concentration dependence of the low-shear viscosity of polyelectrolyte micro-networks: from hard spheres to soft microgels, Europhysics Letters **47**, 729-735 (1999).

[32] M. J. Hernández, J. Pellicer, J. Delegido and M. Dolz, Rheological characterization of Easy-To-Disperse (ETD) Carbopol hydrogels, Journal of Dispersion Science and Technology **19**, 31-42 (1998).

[33] W. W. Graessley, *Polymeric Liquids & Networks: Dynamics and Rheology* (Taylor & Francis Group, New York, 2008).

[34] J. W. Hughes, and R. H. Goodwin, *Rheology for Chemists:An Introduction* (Royal Society of Chemistry, Cambridge, 2000).

[35] Y.-H Lin,. *Polymer Viscoelasticity: Basics, Molecular Theories and Experiments* (World Scientific, New Jersey, 2003).

[36] J. D. Ferry, *Viscoelastic Properties of Polymers* (John Wiley & Sons, New York, 1970).

[37] Q. D. Nguyen, and D. V. Boger, Measuring the flow properties of yield stress fluids, Annual Review of Fluid Mechanics **24**, 47-88 (1992).

[38] P. C. F. Møller, A. Fall, and D. Bonn, No steady state flows below the yield stress. a true yield stress at last? (arXiv:0904.1467v1 [cond-mat.soft] 9 Apr 2009).

[39] C. T. Crowe, *The Multiphase Flow Handbook* (CRC Press, Boca Raton, 2006).

[40] D. J. Durian, and A. J. Liu. Jamming in colloidal dispersions: hard-sphere suspensions, emulsions and foams, in *Jamming and Rheology: Constrained Dynamics on Microscopic and Macroscopic Scales,* edited by A. J. Liu, and S. R. Nagel (Taylor and Francis, London, 2001), pp. 39-49.

[41] A. J. Liu, and S. R. Nagel, Jamming and rheology an introduction, in *Jamming and Rheology: Constrained Dynamics on Microscopic and Macroscopic Scales*, edited by A. J. Liu, and S. R. Nagel (Taylor and Francis, London, 2001), pp. 1-5.

[42] T. G. Mason, M.-D. Lacasse, G. S. Grest, D. Levine, J. Bibette, and D. A. Weitz, Osmotic pressure and viscoelastic shear moduli of concentrated emulsions, Physical Review E **56**, 3150-3166 (1997).

[43] P. Sollich, Rheological constitutive equation for a model of soft glassy materials, Physical Review E **58**, 738-759 (1998).

[44] H. A. Barnes, J. F. Hutton, and K. Waters, *An Introduction to Rheology* (Elsevier, Amsterdam, 1989).

[45] C. G. Robertson, and X. Wang, Isoenergetic jamming transition in particle-filled systems, Physical Review Letters **95**, 075703 (2005).

[46] S. M. Fielding, P. Sollich, and M. E. Cates, Aging and rheology in soft materials, Journal of Rheology **44**, 323-369 (2000).

[47] M. Doi, *Introduction to Polymer Physics* (Clarendon Press, Oxford, 1996).

[48] P.-G. de Gennes,. *Scaling concepts in Polymer Physics* (Cornell University Press, Ithaca, 1979).

[49] P. J. Flory, *Principles of Polymer Chemistry*. (Cornell University Press, Ithaca, 1953).

[50] P.-G. de Gennes, Reptation of a polymer chain in the presence of fixed obstacles, Journal of Chemical Physics **55**, 572-579 (1971).

[51] M. Doi, and S. F. Edwards, *The Theory of Polymer Dynamics* (Clarendon Press, Oxford, 1986).

[52] M. Antonietti, T. Pakula, and W. Bremser, Rheology of small spherical polystyrene microgels: a direct proof for a new transport mechanism in bulk polymers besides reptation, Macromolecules **28**, 4227-4233 (1995).

[53] R. G. Larson, *The Structure and Rheology of Complex Fluids* (Oxford Press, New York, 1999).

[54] B. R. Saunders, and B. Vincent, Microgel particles as model colloids: theory, properties and applications, Advances in Colloid and Interface Science **80**, 1-25 (1999).

[55] I. W. Hamley, *Introduction to Soft Matter* (John Wiley & Sons Ltd., Chichester, 2000).

[56] M. Antonietti, W. Bremser, and M. Schmidt, Microgels: model polymers for the cross-linked state, Macromolecules **23**, 3796-3805 (1990).

[57] R. A. L. Jones, *Soft Condensed Matter* (Oxford University Press, Oxford, 2002).

[58] H. Senff, and W. Richtering, Influence of cross-link density on rheological properties of temperature-sensitive microgel suspensions, Colloid and Polymer Science **278**, 830-840 (2000).

[59] B. E. Rodriguez, M. S. Wolfe, and M. Fryd, Nonuniform swelling of alkali swellable microgels, Macromolecules **27**, 6642-6647 (1994).

[60] M. S. Wolfe, and C. Scopazzi, Rheology of swellable microgel dispersions: influence of crosslink density. Journal of Colloid and Interface Science **133**, 265-277 (1989).

[61] J. Mattsson, H. M. Wyss, A. Fernandez-Nieves, K. Miyazaki, Z. Hu. D. R. Reichman, and D. A. Weitz, Soft colloids make strong glasses, Nature **462**, 83-86 (2009).

[62] M. Cloitre, R. Borrega, F. Monti, and L. Leibler, Structure and flow of poyelectroyte microgels: from suspensions to glasses, Comptes Rendus Physique **4**, 221-230 (2003).

[63] G. Strobl, *The Physics of Polymers* (Springer-Verlag, Heidelberg, 2007).

[64] J. Rička, and T. Tanaka, Swelling of ionic gels: quantitative performance of the Donnan theory, Macromolecules **17**, 2916-2921 (1984).

[65] J. O. Carnali, and M. S. Naser, The use of dilute solution viscometry to characterize the network properties of carbopol microgels, Colloid and Polymer Science **270**, 183-193 (1992).

[66] M. K. Nagarajan, and H. Ambuter, Polymeric stabilizers for liquid detergents, in *Liquid Detergents*, edited by K.-Y. Lai (Marcel Dekker, New York, 1997), pp. 129-177.

[67] P. Reeve, T. Tepe, and J. Shulman, Rheology modifiers and thickeners for liquid detergents, in *Liquid Detergents*, 2nd ed., edited by K.-Y. Lai (CRC Press, Boca Raton, 2006), pp. 113-144.

[68] D. Benda, J. Šňupárek, and V. Čermák, Inverse emulsion polymerization of acrylamide and salts of acrylic acid, European Polymer Journal **33**, 1345-1352 (1997).

[69] W. N. Charman, D. P. Christy, E. P. Geunin, and D. C. Monkhouse, Interaction between calcium, a model divalent cation, and a range of poly(acrylic acid) resins as a function of solution pH, Drug Development and Industrial Pharmacy **17**, 271-280 (1991).

[70] B. W. Barry, and M. C. Meyer, The rheological properties of Carbopol gels I. continuous shear and creep properties of Carbopol gels, International Journal of Pharamaceutics **2**, 1-25 (1979).

[71] F. K. Oopong, and J. R. de Bruyn, Microrheology and jamming in a yield-stress fluid, In Preparation.

[72] A. M. V. Putz, and T. I. Burghelea, The solid-fluid transition in a yield stress shear thinning physical gel, Rheological Acta **48**, 673-689 (2009).

[73] P. H. T. Uhlherr, J. Guo, C. Tiu, X.-M. Zhang, J. Z.-Q. Zhou, and T.-N. Fang, The shear-induced solid-liquid transition in yield stress materials with chemically different structures, Journal of Non-Newtonian Fluid Mechanics **125**, 101-119 (2005).

[74] F. K.Oopong, and J. R. de Bruyn, Diffusion of microscopic tracer particles in a yield-stress fluid, Journal of Non-Newtonian Fluid Mechanics **142**, 104-111 (2007).

[75] B. R. Dasgupta, S.-Y. Tee, J. C. Crocker, B. J. Frisken, and D. A. Weitz, Microrheology of polyethylene oxide using diffusing wave spectroscopy and single scattering, Physical Review E **65**, 051505 (2002).

[76] B. R. Dasgupta, and D. A. Weitz, Microrheology of cross-linked polyacrylamide networks, Physical Review E **71**, 021504 (2005).

[77] D. D. Desai, D. F. Hasman, J. F. Schmucker-Castner, Advances in carbomer polymer technology, Cosmetics and Toiletries Manufacture Worldwide **107**, 81-94 (1992).

[78] D. Lee, *Structural Investigation of Carbopol ETD 2050 by Light Scattering* (Simon Fraser University, Burnaby, 2009).

[79] P. Coussot, L. Tocquer, C. Lanos, and G. Ovarlez, Macroscopic vs. local rheology of yield stress fluids, Journal of Non-Newtonian Fluid Mecahnics **158**, 85-90 (2009).

[80] B. Chu, *Laser Light Scattering: Basic Principles and Practice* (Academic Press Inc., San Diego, 1991).

[81] T. G. Mason, and M. Y. Lin, Density profiles of temperature-sensitive microgel particles, Physical Review E **71**, 040801 (2005).

[82] K. Hyun, S. H. Kim, K. H. Ahn, and S. J. Lee, Large amplitude oscillatory shear as a way to classify the complex fluids, Journal of Non-Newtonain Fluid Mechanics **107**, 51-65 (2002).

[83] T. Freltoft, J. K. Kjems, and S. K. Sinha, Power-law correlations and finite-size effects in silica particle aggregates studied by small-angle neutron scattering, Physical Review B **33**, 269-275 (1986).

[84] J. Teixeira, Small-angle scattering by fractal systems, Journal of Applied Crystallography **21**, 781-785 (1988).

[85] H. H. Winter, P. Morganelli, and F. Chambon, Stoichiometry effects on rheology of model polyurethanes at the gel point, Macromolecules **21**, 532-535 (1988).

[86] G. Beaucage, Small-angle scattering from polymeric mass fractals of arbitrary mass-fractal dimension, Journal of Applied Crystallography **29**, 134-146 (1996).

[87] A. N. Falcão, J. S. Pedersen, and K. Mortensen, Structure of randomly cross-linked poly(dimethylsiloxane) networks produced by electron irradiation, Macromolecules **26**, 5350-5364 (1993).

[88] B. W. Barry, and M. C. Meyer, The rheological properties of Carbopol gels II.oscillatory properties of Carbopol gels, International Journal of Pharmaceutics **2**, 27-40 (1979).

[89] T. McLeish, Rheolgy of linear and branched polymers, in *Soft and Fragile Matter: Nonequilibriun Dynamics, Metastability and Flow*, edited by M. E. Cates, and M. R. Evans (Institute of Physics Publishing, Bristol, 1999), pp. 79-111.

[90] P. Coussot, H. Tabuteau, X. Chateau, L. Tocquer, and G. Ovarlez, Aging and solid or liquid behaviour in pastes, Journal of Rheology **50**, 975-994 (2006).

[91] P. A. M. Steeneken, Rheological properties of aqueous suspensions of swollen starch granules, Carbohydrate Polymers **11**, 23-42 (1989).